Abstract

Analysis of Faradaic Reaction and Its Effect on Desalination Performance in Capacitive Deionization

Jihyun Yu

School of Chemical and Biological Engineering

The Graduates School

Seoul National University

Capacitive deionization (CDI) is a desalination technique that removes salt from the saline water, applying a potential difference between two porous activated carbon electrodes. Membrane assisted CDI (MCDI) is a commonly used system that improves performance by installing an ion exchange membrane in the CDI system. CDI is mainly known to be deionized by Non Faradaic reaction, but recently there have been limited reports on H_2O_2 generation, pH change and oxidation of carbon electrode in relation to Faradaic reaction. Therefore, the detailed study of Faradaic reaction characteristics in CDI and MCDI systems is required.

The purpose of this study is to investigate the characteristics of the Faradaic reaction and the quantitative effect on the desalination performance in flow-mode CDI and MCDI systems. As major results, firstly, the H_2O_2 formation and effluent pH change in case of MCDI ($[H_2O_2]$ = 5.5 μM) were much smaller than that of CDI (37.0 μM), indicating the less occurrence of Faradaic reactions for MCDI. However, the surface pH of carbon electrode in the MCDI was much more acidic (pH ~1.5) at the anode and more basic at the cathode (pH ~ 11.7), indicating the deterred transfer of byproducts (OH^- and H^+) generated in the compartment inside of ion change membrane. In addition, the quantitative analysis regarding the extent of Faradaic reaction between these two systems were provided based on measured byproducts. Secondly, the long-term study indicated that the performance reduction of deionization in MCDI (17%) was much smaller than that of CDI (85%), which can be supported by their asymmetrically oxidized anode analyzed by FT-IR, CV, and XPS. In addition, the strategies to overcome the performance reduction by coating the carbon electrode with ion exchange polymer or applying alternate reverse potential were suggested. Finally, the deep understanding about Faradaic reactions affecting short-term or long-term CDI performance can ultimately contribute to the development of CDI performance and long-term stability.

Keywords: capacitive deionization, desalination, Faradaic reaction, pH distribution, H_2O_2 generation, carbon electrode oxidation, charge consumption

Student Number: 2010-24100

Tables of contents

List of Figures

List of Tables

1. Introduction

1.1. Backgrounds

Capacitive deionization (CDI) has recently received much attention as a desalination process [2-6]. CDI desalinates brackish water when passed between two porous electrodes, mostly made of activated carbons, by applying an electrical potential. CDI consists of two main processes, charging and discharging processes. In the charging step, ions are attracted and stored on the electrode surface as forming electrical double layer, and consequently, the solution passing between the electrodes can be desalinated [7-11]. In the followed discharge step, the stored ions are released by shorting or reversing the potential, and therefore the electrodes can be regenerated. MCDI (Membrane assisted CDI) is one of the widely used CDI systems, additionally install ion-exchange membranes between the electrodes, showing high desalination performance and long-term stability [12-14]. It was reported that the ion-exchange membrane or coating of the ion-exchange resin decreases the co-ion repulsion and increases the adsorption performance [15-19]. CDI and MCDI are an electrochemically driven process in which a non-Faradaic reaction intended process controls the desalination process. Therefore, the appropriate operation is required to achieve efficient desalination without any undesirable energy loss.

To avoid unwanted Faradaic reactions for an energy-efficient process, the applied potential has been typically limited to 1.2 V [5, 20-22] because the electrolysis of

water is negligible in this potential range. However, unexpected side reactions have been reported in an early CDI study [5] even when the applied potential was kept below 1.2 V. Incomplete decay of the current was proposed as evidence for parasitic electrochemical reactions together with current leakage. Afterwards, several Faradaic reactions were postulated by altering the applied potential and following the pH changes [23]. Reduction of dissolved oxygen (pH increase) and oxidation of the carbon electrodes (pH decrease) were suggested as possible explanations for the pH changes during the process. Another study revealed that dissolved oxygen (DO) could be involved in the side reactions by observing the cumulative charge and pH changes with and without nitrogen purging [24]. Changes of pH was also examined using a three electrode system by varying applied potentials [25]. Increasing the applied voltage above 1.2 V caused more side reactions, which decreased the effluent pH below 5 and induced discrepancy between effluent conductivities and ion concentrations [26]. Previous studies have reported that the oxidation of the carbon at the anode can occur at over 0.7 - 0.9 V of applied potential [23, 27], which resulted in oxidation of the electrode surface over a long term operation. Oxidation of the carbon electrode can cause deterioration of the long-term performance by changing the electrochemical characteristics of the electrode [13, 24, 28]. The change of electrochemical characteristics of the oxidized electrode have been found through the increase of oxygen content and the change of potential of zero charge of the electrode [13, 25, 29].

On the other hand, Faradaic reactions in the cathode have been poorly investigated; several electrochemical reactions related to the reduction of DO were suggested to explain the effluent pH fluctuations [23-25]. Recently, Faradaic reactions in a batch-mode CDI and MCDI was examined, which reported produced H_2O_2 and decreased DO concentrations [30, 31]. However, such measurements were performed only in a batch-mode system. In addition, although more studies the evidences of Faradaic reaction in the CDI system have been steadily reported [32, 33], the analysis of Faradaic reactions and interpretation of the effect of Faradaic reaction on deionization capacity are limited in CDI, MCDI, and even in long-term systems.

1.2. Objectives

The purpose of this study is to analyze temporal and spatial Faradaic reactions and interpret the deionization performance with Faradaic reaction besides of adsorption/desorption capacity. The characteristics and effects of Faraday reaction in CDI and MCDI systems were compared and analyzed in short and long-term operations.

Firstly, in short term operation of CDI and MCDI, the characteristics of Faradaic reaction were analyzed and the effect of the Faradaic reaction on deionization capacity was interpreted based on the results. For this, the pH distribution in the effluent and the surface and the generated H_2O_2 were measured in flow-mode CDI and MCDI systems. The effect of the spatial distribution of Faradaic reaction products on the salt adsorption capacity and the development of additional Faradaic reactions was also compared in both systems. Appropriate Faradaic reactions at anode and cathode were proposed based on the electrode working potential and locally distributed surface pH.

Secondly, in long-term operation of CDI and MCDI, the changes of Faradaic reaction property was analyzed and the decrease in deionization performance was interpreted from the effects of Faradaic reaction and by-products of reaction. For this, effluent conductivity, effluent H_2O_2 concentration, effluent pH, and electrode working potentials were continuously measured during long-term

operation. Also, the electrochemical properties of long-term cycled electrodes were analyzed by the potential of zero charge (E_{pzc}), FT-IR, and XPS. The charge consumption for Faradaic reaction and co-ion repulsion was newly calculated based on the measured Faradaic reaction products in both systems.

2. Literature review

2.1. CDI and MCDI

Currently, human beings are faced with water depletion problem, and as a technical method to solve this, a process of desalinating brackish or sea water is being watched. Although the reverse osmosis (RO) process is the most widely used desalination technology in the world, it requires a high presser, which is very disadvantageous in terms of energy efficiency [7]. Recent interest in the CDI process has been amplified by the benefits of higher energy efficiency at low salinity and lower material and operating costs compared to RO [7, 34-36]. CDI is a desalination technique that removes salt from saline water, applying a potential difference between two porous activated carbon electrodes [2-6, 18]. The dissolved ions form an electric double layer with the electrode surface (Figure 2-1) and removed from the water (Figure 2-2) [7-11].

The process of the capacitive desalination technology consist of charging and discharging steps, as shown in Figure 2-3. In the charging process, electric energy is applied to adsorb ions in the pores. After the ions are saturated in the pores, electric energy is reduced or shorted to release ions and the electrode is regenerated. In general CDI operation, the charging process operates at an applied potential that is lower than 1.23V (vs. NHE), where no water electrolysis occurs [5, 7, 37]. Because CDI removes ions from the formation of electrical double layers, deionization capacity can be maximized in the absence of Faradaic reaction.

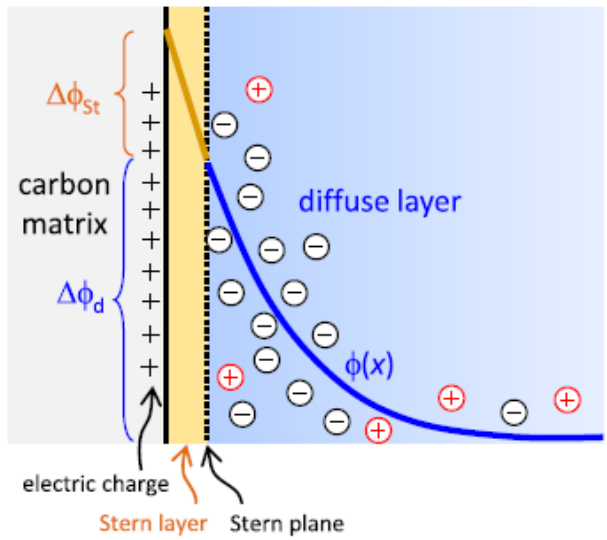

Figure 2-1. Electrical double layer (EDL) formed on porous electrode surface according to Gouy–Chapman–Stern model [2].

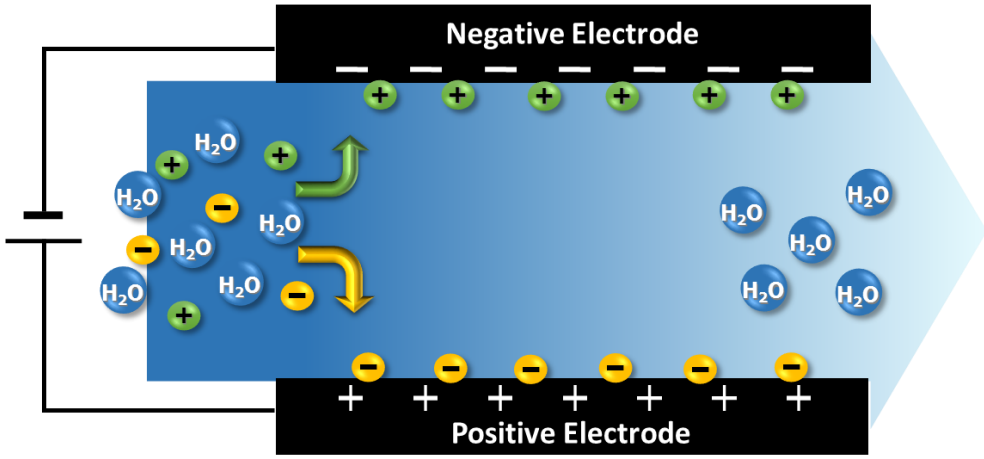

Figure 2-2. A schematic of capacitive deionization (CDI) process.

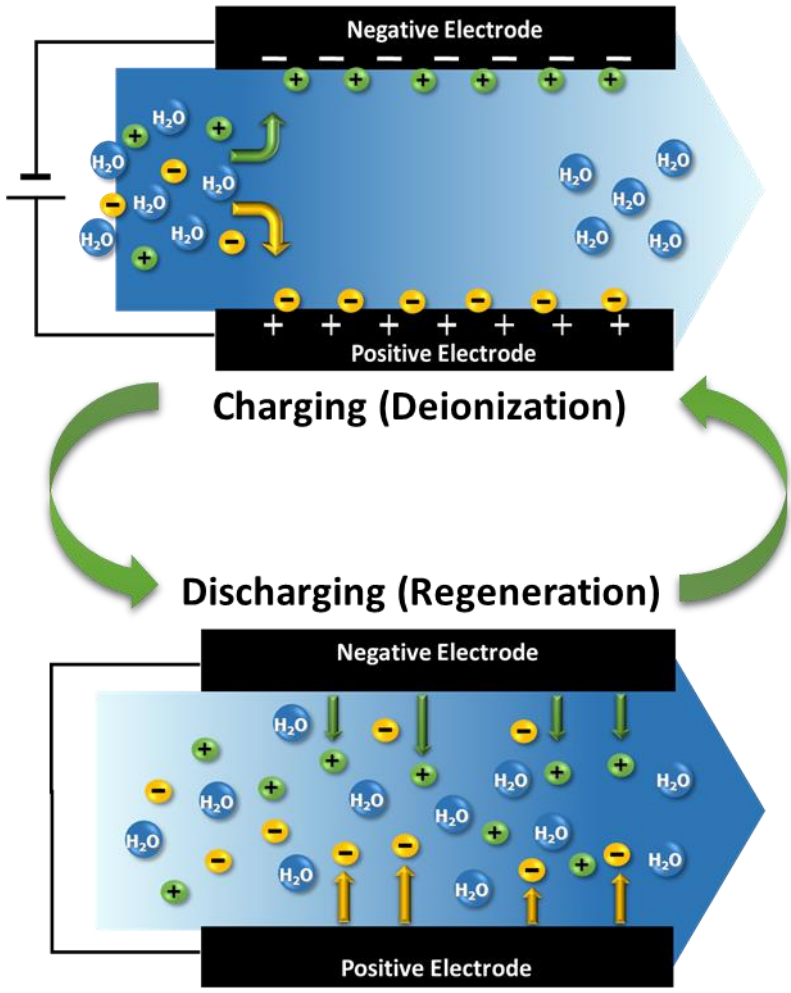

Figure 2-3. A schematic diagram of the charge and discharge step of CDI.

In order to increase the ion removal performance in CDI, development of technologies such as electrodes, systems, and operations has been actively pursued. Among them, MCDI, as a system development, added ion exchange membrane to existing CDI system cell to greatly improve ion removal performance and is the most widely used CDI system recently (Figure 2-4) [14-17]. An anion exchange membrane is installed on the surface of the negative electrode (cathode) while a cation exchange membrane is installed on the surface of the positive electrode (anode). On the negatively charged surface of the cathode, the anion is blocked by the cation exchange membrane and only the cation can freely move through the membrane, so that the adsorption and storage of the cation can be performed without the influence of the anion. The opposite phenomenon occurs in the positively charged electrode (Figure 2-5). Therefore, in MCDI, where the movement of co-ions are restricted, the BC region can be minimized in Figure 2-6, so the charge efficiency and the adsorption amount of ions increase (Figure 2-7). In addition, a reverse polarization for electrode regeneration is possible in MCDI system. In CDI, when the reverse potential is applied, the adsorption of ions is directed to the opposite electrode, so that desorption and re-adsorption of ions occur simultaneously. However, in the case of MCDI, the adsorption of ions can be performed in only one direction by the ion exchange membrane, so that adsorption phenomenon cannot occur even when the reverse potential is applied. Therefore, electrode can be regenerated by the discharging of reverse polarization in MCDI. Although the discharging of reverse polarization increases energy

consumption, the required time for ion desorption is shortened and the desorption is ensured, so that the amount of ion adsorption in the next step can be increased.

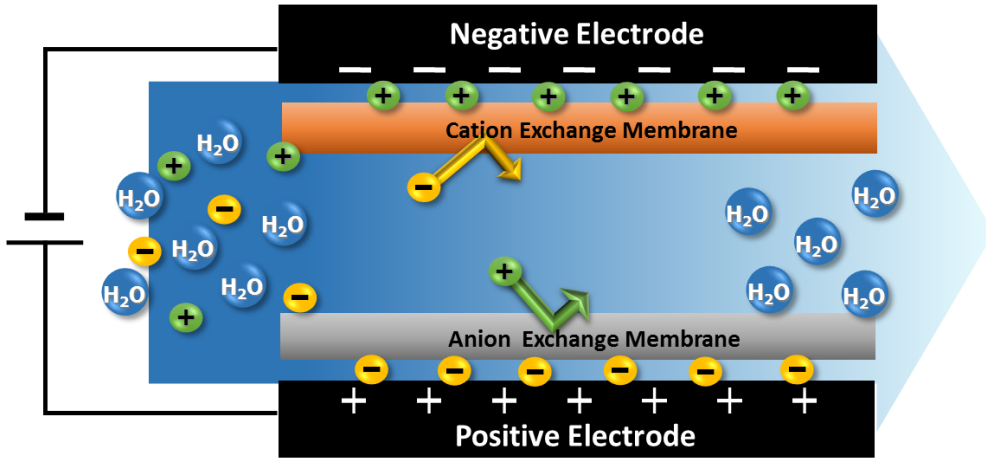

Figure 2-4. A schematic of Membrane assisted CDI (MCDI).

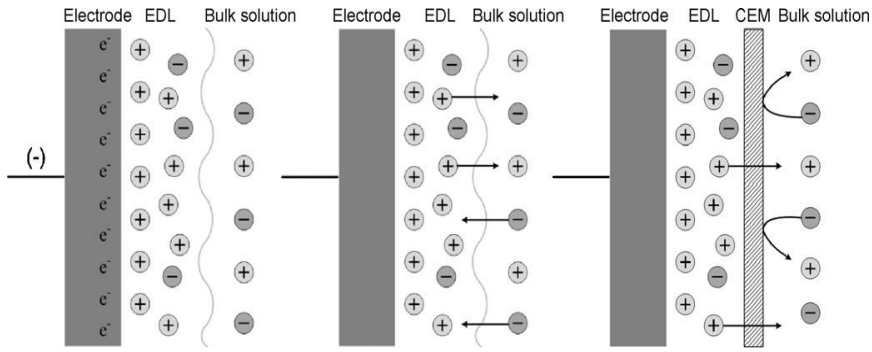

Figure 2-5. The distribution and transport of ions at the electrode surface in MCDI [1].

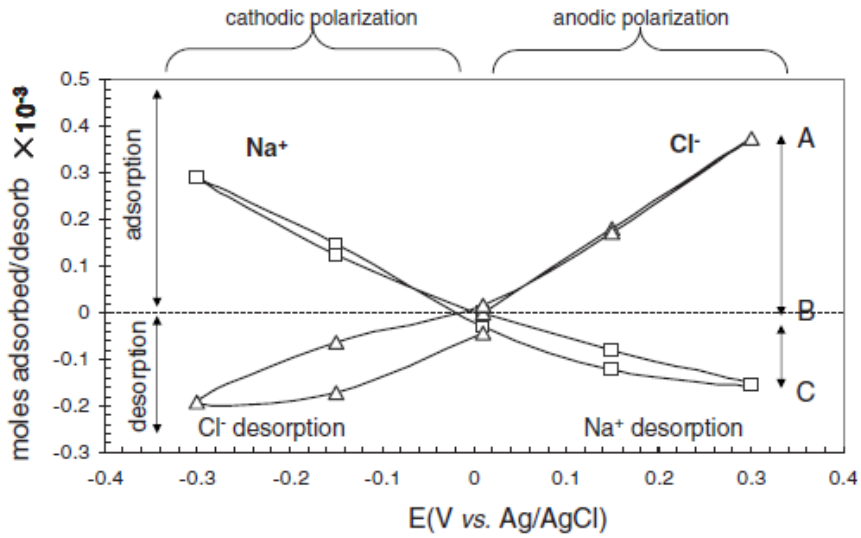

Figure 2-6. The amounts of Na^+ cation and Cl^- anion adsorption and desorption to the carbon electrodes, when the electrode is polarized to 0.3 V vs Ag/AgCl [38].

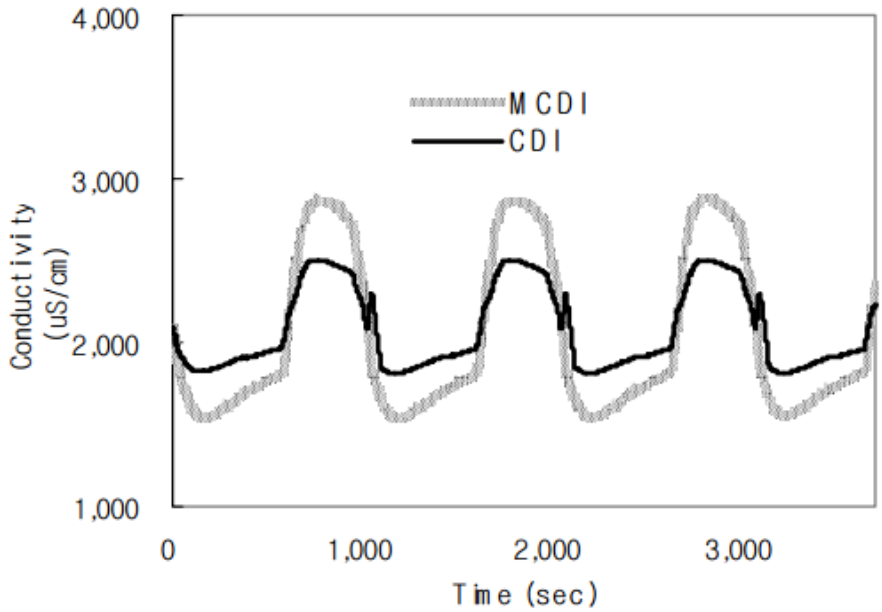

Figure 2-7. Improvement of ion adsorption during charging step (decrease in conductivity) and desorption during discharging step (increase in conductivity) in MCDI compared to CDI [12].

2.2. Faradaic reactions

In order to prevent side reactions that reduces the ion adsorption efficiency, CDI system is operated at a potential lower than 1.23 V that electrolysis of water occurs [23, 27]. However, despite the CDI system driving voltage of 1.2 V of less, it was suspected that undesirable Faraday reactions occurred [24, 25]. Figure 2-8 shows a timeline of the studies related to Faradaic reactions and long-term stability in CDI. Firstly, one of the evidences of side reactions occurring in the CDI system is the effluent pH fluctuation [23, 24, 39]. As shown in Figure 2-9, the pH initially increased and then decreased during the charging process. The higher the applied potential, the larger the fluctuation width. Figure 2-10 shows the change of effluent pH in the presence/absence of oxygen and applied potential. The pH fluctuation was less in the system which cut off the oxygen supply. Therefore, it is reported that the DO is related to the side reaction occurring in CDI, and the pH of the effluent is changed by the side reaction.

$$O_2 + H_2O + 4e^- \rightarrow 4OH^-,\ E^0 = 0.207\ V \quad (2\text{-}1)$$

$$O_2 + H_2O + 2e^- \rightarrow HO_2^- + OH^-,\ E^0 = 0.065\ V \quad (2\text{-}2)$$

$$HO_2^- + 2H_2O + 2e^- \rightarrow 3OH^-,\ E^0 = 0.867\ V \quad (2\text{-}3)$$

DO is reduced to generate OH^- at the cathode as follows the Reaction (2-1), (2-2), or (2-3), and reverse reactions can occur at anode [23].

Also, in the Figure 2-11, the accumulated charge is increased in a cycle by the loss of charge and it decreased with lower applied potential. The different magnitude of charge between charging and discharging step may due to the presence of side reaction in addition to the adsorption/desorption of ions [39].

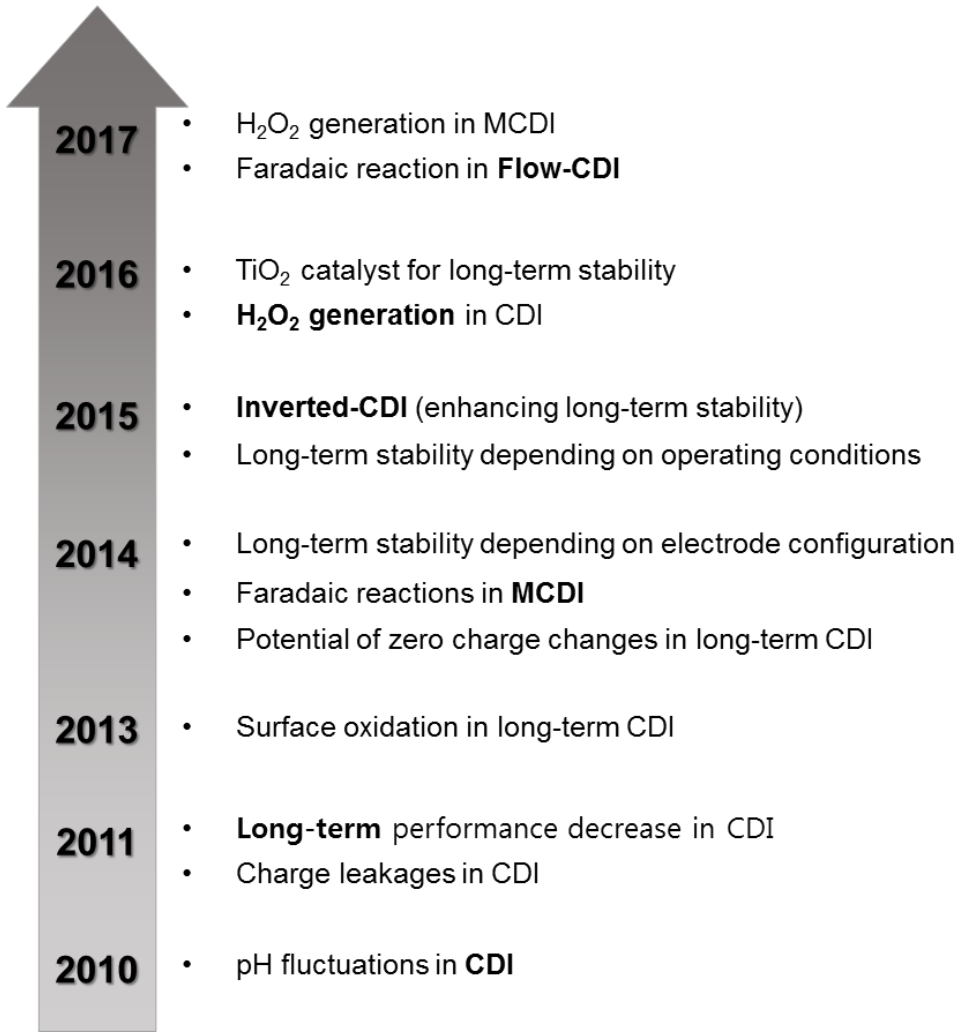

Figure 2-8. A timeline of the studies related to Faradaic reactions and long-term stability in CDI.

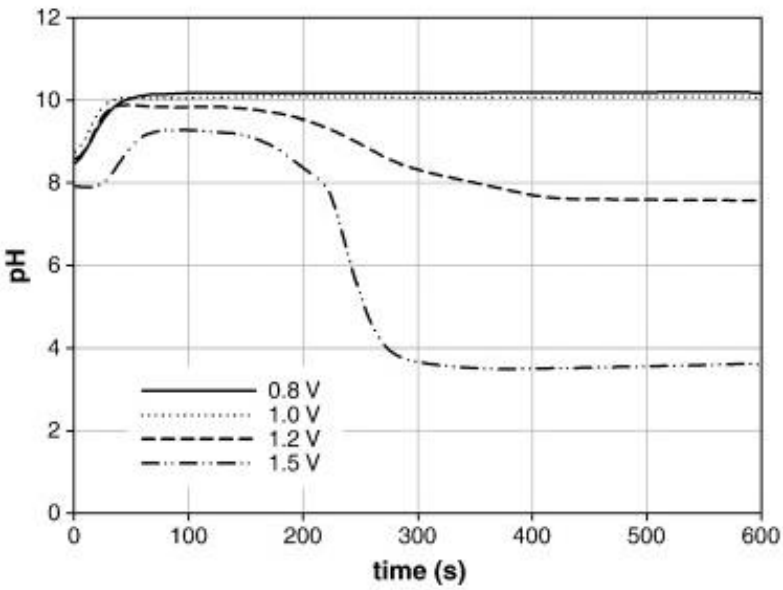

Figure 2-9. pH fluctuation of CDI treated water at various applied potentials [23].

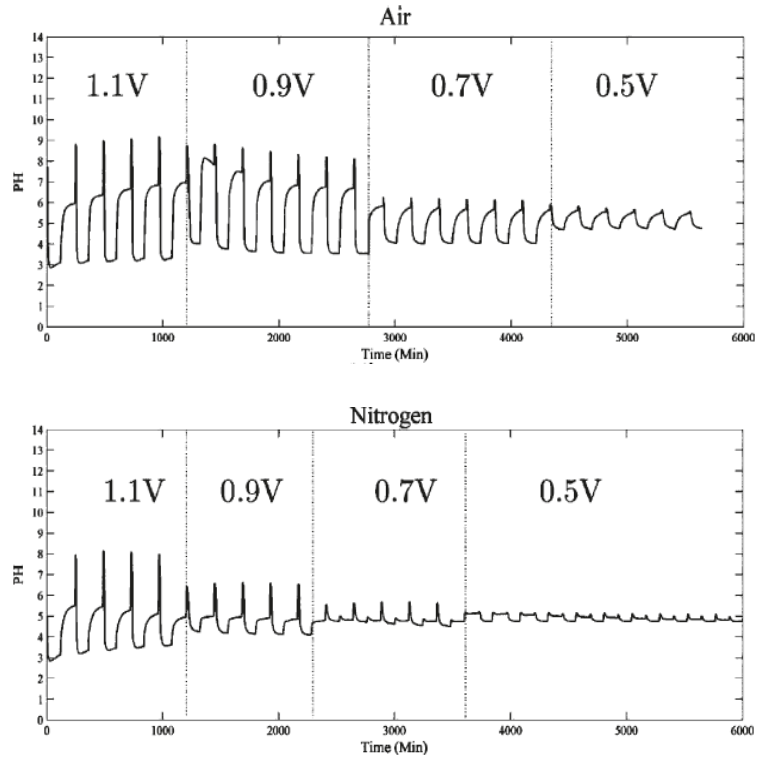

Figure 2-10. Change of effluent pH in the presence/absence of oxygen and applied potential [24].

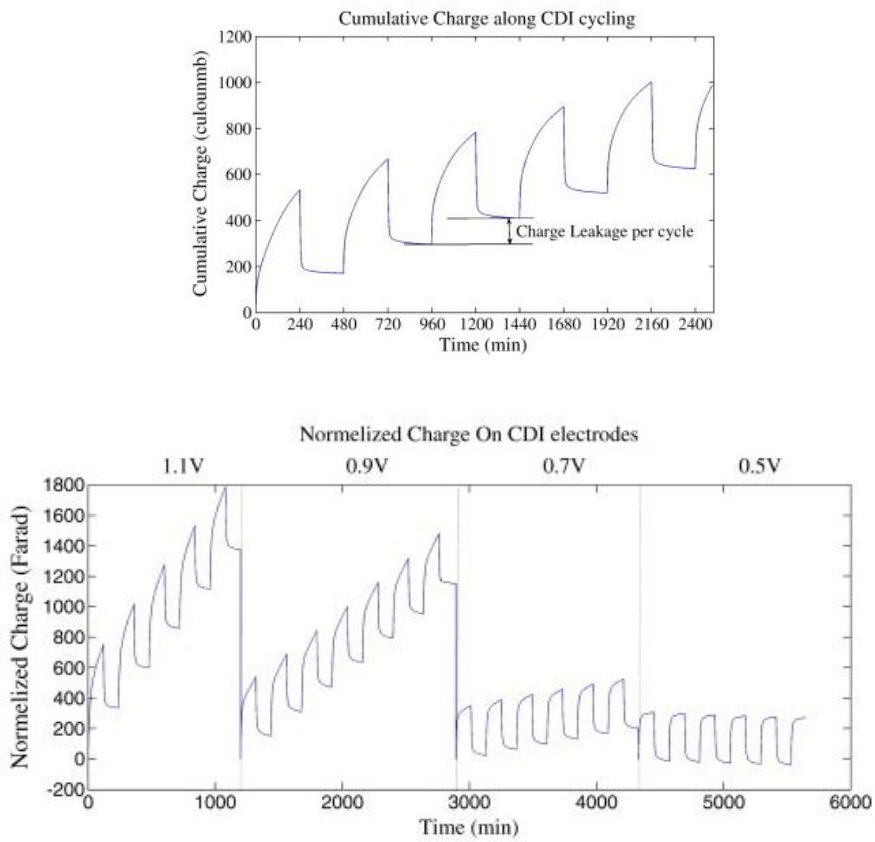

Figure 2-11. Cumulative charge at the different applied potential in CDI system [39].

The Faradaic reactions can lead to the oxidation of carbon at the anode. The oxidation of carbon electrode was early reported in the field of fuel cell. The production of carbon dioxide by oxidation of carbon can occur thermodynamically at a potential higher than 0.207 V (vs. NHE) and at a higher potential than 0.518 V for carbon monoxide production [40].

$$C + 2H_2O \rightarrow CO_2 + 4H^+ + 4e^-,\ E^0 = 0.207\ V \quad (2\text{-}4)$$

$$C + H_2O \rightarrow CO + 2H^+ + 2e^-,\ E^0 = 0.518\ V \quad (2\text{-}5)$$

$$CO + H_2O \rightarrow CO_2 + 2H^+ + 2e^-,\ E^0 = -0.103\ V \quad (2\text{-}6)$$

Figure 2-12 shows an increase in the corrosion rate above about 0.9 V, probably due to the oxidation of carbon by Reaction (2-4) and (2-5). At potentials above 0.207 V, oxygen functional groups can be generated on the carbon (2-7), and this irreversible intermediate oxidation can lead to carbon dioxide formation (Reaction (2-8)) at the higher potentials.

$$C + H_2O \rightarrow C\text{–}O_{ad} + 2H^+ + 2e^-,\ E^0 = 0.207\ V \quad (2\text{-}7)$$

$$C\text{–}O_{ad} + H_2O \rightarrow CO_2 + 2H^+ + 2e^- \quad (2\text{-}8)$$

It is also assumed that the oxidation peak of carbon in Figure 2-12, which occurs largely in the reducing potential region in the air condition (I), is due to hydrogen peroxide. At the carbon electrode, oxygen is converted to hydrogen peroxide by two electron transfers [41]. The generated hydrogen peroxide or hydrogen peroxide radical can oxidize the carbon as following reactions.

$$C + H_2O_2 \rightarrow C–O_{ad} + H_2O \quad (2\text{-}9)$$

$$C–O_{ad} + H_2O_2 \rightarrow CO_2 + H_2O \quad (2\text{-}10)$$

Electrochemical or chemical corrosion of carbon increases the defects of carbon and oxide groups on the surface. The oxygen and hydrogen functional groups that can occur in the carbon structure are shown in Figure 2-13 [42]. Carbon oxidation, which begins with the generation of oxygen functional groups, can occur from where there are unsaturated bonds and free electrons at the corner or edge.

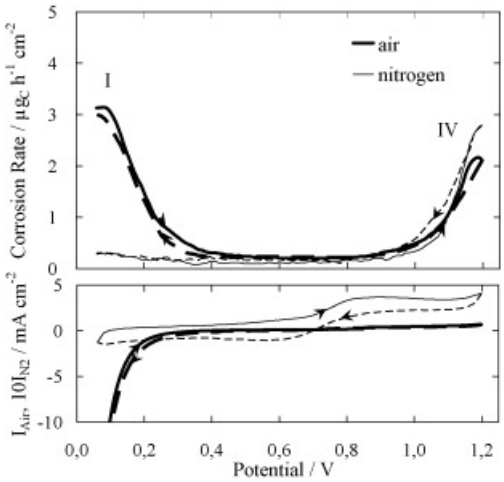

Figure 2-12. Potentiodynamic corrosion rate in nitrogen and air conditions. Figure above: total carbon corrosion rate obtained by a sum of carbon dioxide and carbon monoxide generation. Figure below: corresponding currents [40].

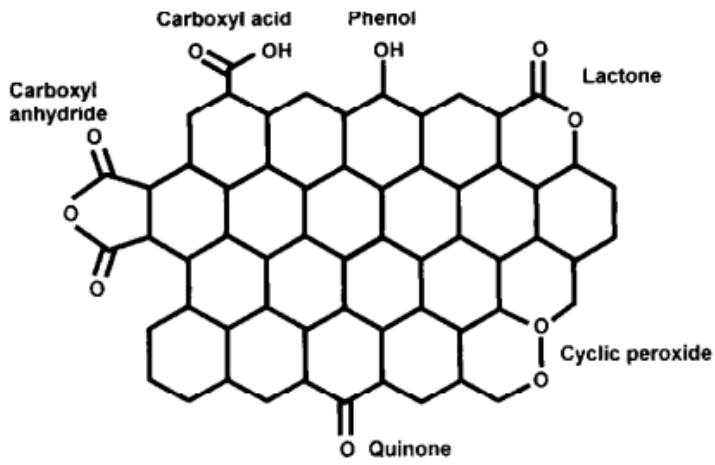

Figure 2-13. Oxygen functional groups on activated carbon surface [42].

In CDI, the oxidized surface has been also found on the anode through the increase of oxygen content and the change of potential of zero charge of the electrode after long-term operation [13, 25, 29]. Figure 2-14 shows the XPS spectra of the electrode surface which was operated for about 200 hr at 0.9/0 V applied potential [25]. After the long-term operation, the content of oxygen element in the anode surface increased significantly compared to the initial state. Figure 2-15 shows the change of surface functional group from FTIR spectra of anode and cathode after long-term operation [13]. In case of anode, COOH group was newly generated at the wavenumber of 1730 cm^{-1}. Therefore, it can be seen that surface changes such as formation of functional groups including oxygen are accompanied by long-term operation. Especially, the change of the surface was larger in the anode. This is probably due to the oxidation of the surface carbon by the oxidation reaction at the anode.

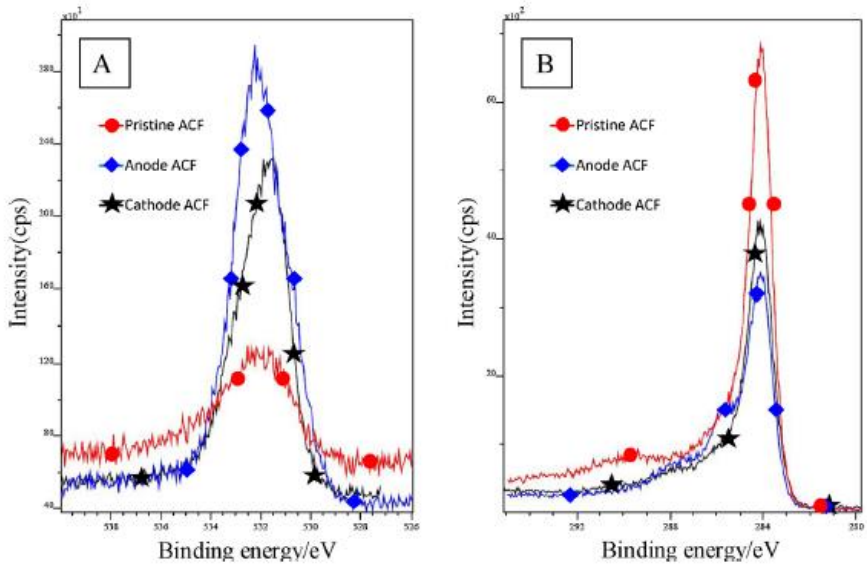

Figure 2-14. XPS spectra of the electrode surface which was operated for about 200 hr at 0.9/0 V applied potential (A) oxygen peak (O 1s), (B) carbon peak (C 1s) [25].

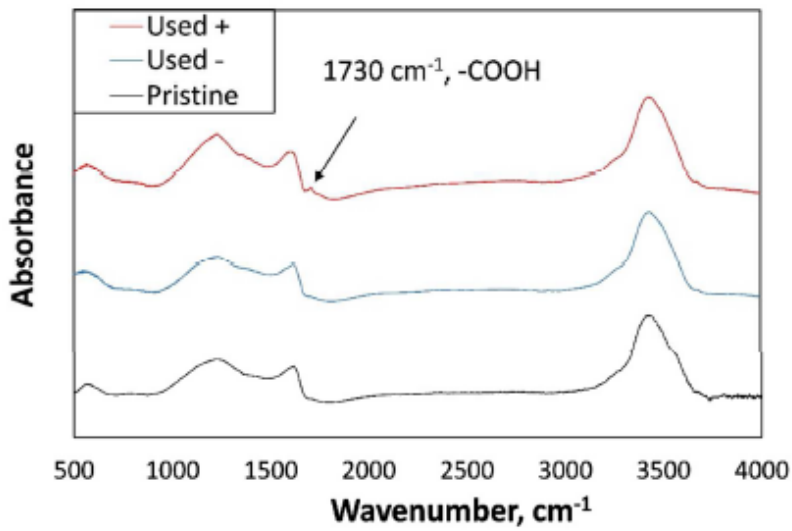

Figure 2-15. FTIR spectra of the used anode (Used +) and cathode (Used -) after long-term operation in comparison with the pristine electrode [13].

Changes in surface functional groups affect electrochemical properties such as surface charge. The newly created oxygen functional groups on the surface, especially functional groups such as COO^-, are negatively charged and positively shift the potential of zero charge (E_{pzc}) of the electrode. The E_{pzc} of the electrode is the potential at which the net charge on the surface is zero, so the absolute value of the current in cyclic voltammetry (CV) and the capacity value in the electrochemical impedance spectroscopy (EIS) are minimal [43].

Figure 2-16 shows the CV results of the long-term operated anode and cathode in CDI. When E_{pzc} is deduced from CV, it can be seen that the negative electrode has not changed much compared to the pristine (~ 0.0 V vs. SCE), whereas the positive electrode has been shifted to positive (~ 0.4 V vs. SCE). Also, Figure 2-17 shows the results of the EIS of the long-term operated anode and cathode in CDI. The electrode potential when the capacitance is the minimum (E_{pzc}) is not greatly changed in cathode, but it is shifted to 0.2 V after 25 cycles and about 0.4 V after 50 cycles in anode. This indicates that as the operation progresses, the oxidation of the anode is intensified, thus the E_{pzc} of the anode shifts more and more positively.

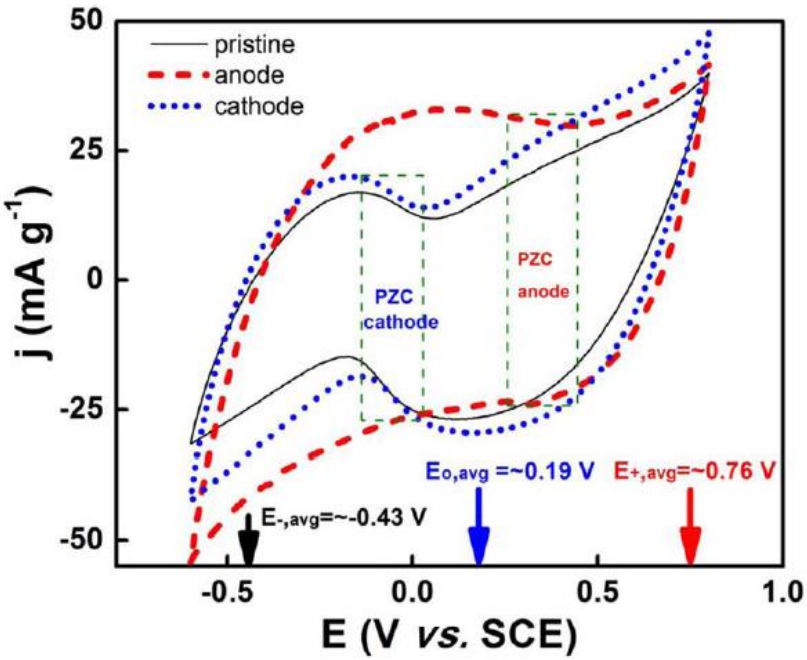

Figure 2-16. Cyclic voltammetry of long-term operated anode and cathode operated at 1.2/0 V for 248 cycles (1 mV/s, 4.3 mM NaCl solution) [44].

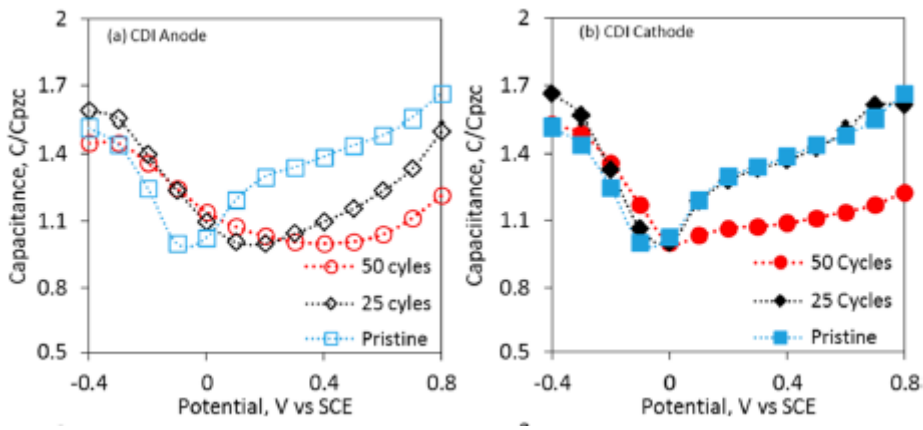

Figure 2-17. EIS differential capacity of long-term operated anode and cathode at 1.2/0 V (0.01 M NaCl, 0.2 Hz) [13].

The Faradaic reactions not only changes the surface properties of the electrode but also can change the working potential of the electrode during long-term operation. In the early stage, the anode and cathode have almost equal potential distributions, but in the long-term stage, more voltage is applied to the anode and the unbalanced distribution of potential between anode and cathode is obtained [24, 25, 29]. Figure 2-18 shows the working potential of anode and cathode in long-term operated CDI system[24]. At an applied potential of 0.9 V, the electrode working potential distribution of anode is about 0.55 V, which is higher than that of cathode (0.35 V). It was explained that a current leakage occurs due to some Faradaic reaction (e.g., oxygen reduction at the cathode), and thus a relatively higher voltage is applied to the anode side. It was also explained that the oxidation of carbon was sufficiently enabled as the working potential distribution of the anode increased.

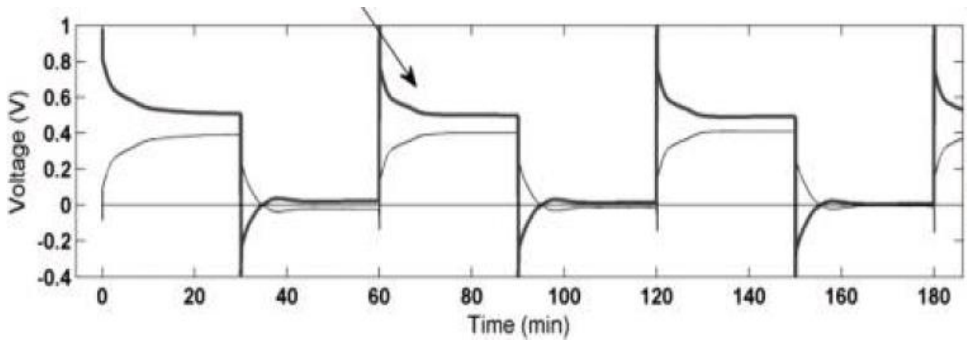

Figure 2-18. The working potential distribution between anode and cathode in long-term operated CDI system at 0.9/0V (Bold solid: anode (~ 0.55 V), solid: cathode (~ 0.35 V)) [24].

2.3. Performance in long-term operation

The changes of electrochemical properties of electrodes by Faradaic reactions can affect deionization performance in the long-term CDI [28, 45, 46]. In the long-term operation, deionization performance is deteriorated as shown in the following Figure 2-19. As the CDI operation time passes, the decrease of conductivity during ion adsorption and the increase of conductivity during ion desorption gradually decreased. This means that the ion adsorption and desorption capacity of the electrodes are lower than those at the initial stage. What is also interesting is that at the beginning of adsorption, there is a region where desorption of ions predominates (inversion peak) as shown in Figure 2-20. In addition, adsorption occurs in which the conductivity decreases even during the discharging step.

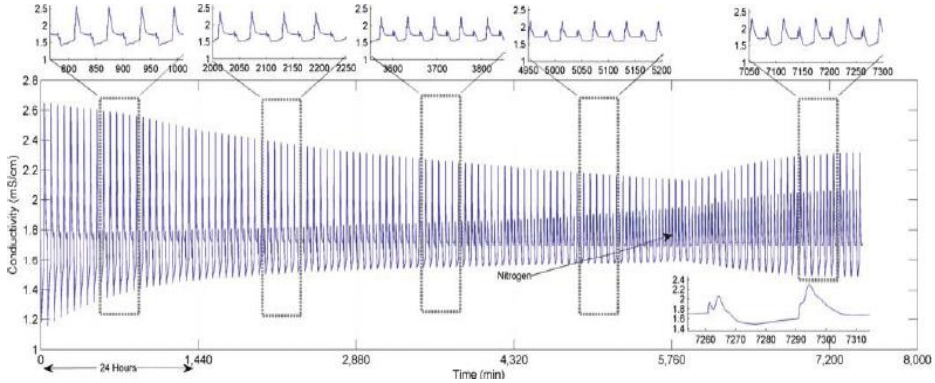

Figure 2-19. The change of conductivity over time in 0.9/0 V applied long-term CDI operation [24].

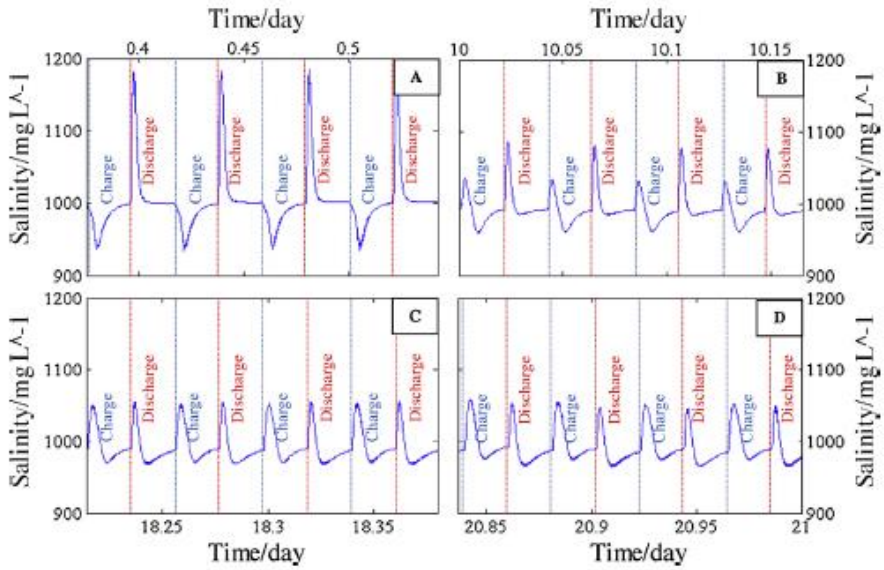

Figure 2-20. The change of salinity over time in long-term CDI long-term. From the stage of B, the inversion peak was shown at the beginning of the charge [28].

The deterioration of the salt adsorption performance can be explained from the electrochemical changes of the electrode properties such as E_{pzc} and working potential in the long-term operation [38, 44, 47, 48]. Basically, when an electric potential higher than E_{pzc} is applied to the electrode, the anion adsorbs predominantly. On the contrary, when the electric potential lower than E_{pzc} is applied, the cation adsorbs predominantly. Figure 2-21 shows the change of ion adsorption and desorption characteristics of electrode according to E_{pzc} change by chemical treatment (acidification by HNO_3) for surface oxidation. For example, when the same positive potential (+0.3 V vs. Ag/AgCl) was applied to the electrode in Figure 2-21a, the anion adsorbed on the pristine electrode (E_{pzc}=0 V), while the oxidized electrode (E_{pzc}=0.35 V) is predominant in cation adsorption. Figure 2-22 is an illustration to interpret the deterioration of salt adsorption capacity in prolonged CDI operation with the changes of E_{pzc} and working potential of the two electrodes. In the early stage (a), since the working potential distribution of the two electrodes is relatively balanced between E_{pzc}, the adsorption of anions on the positive electrode and the adsorption of positive ions on the negative potential are predominant, so ion adsorption can be actively performed. However, as the operation progresses (b), anion adsorption decreases as E_{pzc} of the anode shifts to positive, and cation adsorption decreases as the working potential region positively increased at the cathode. In the prolonged operation (c), the cation adsorption capacity is greatly reduced as the potential distribution of the cathode is reduced, and the E_{pzc} further shifts to positive at the

anode, resulting in an electrode state favorable for the adsorption of the cation. Therefore, in the discharging step, the anode adsorbs cations and, on the contrary, desorbs the adsorbed cations in the charging step and exhibits desorption peaks (inversion peak).

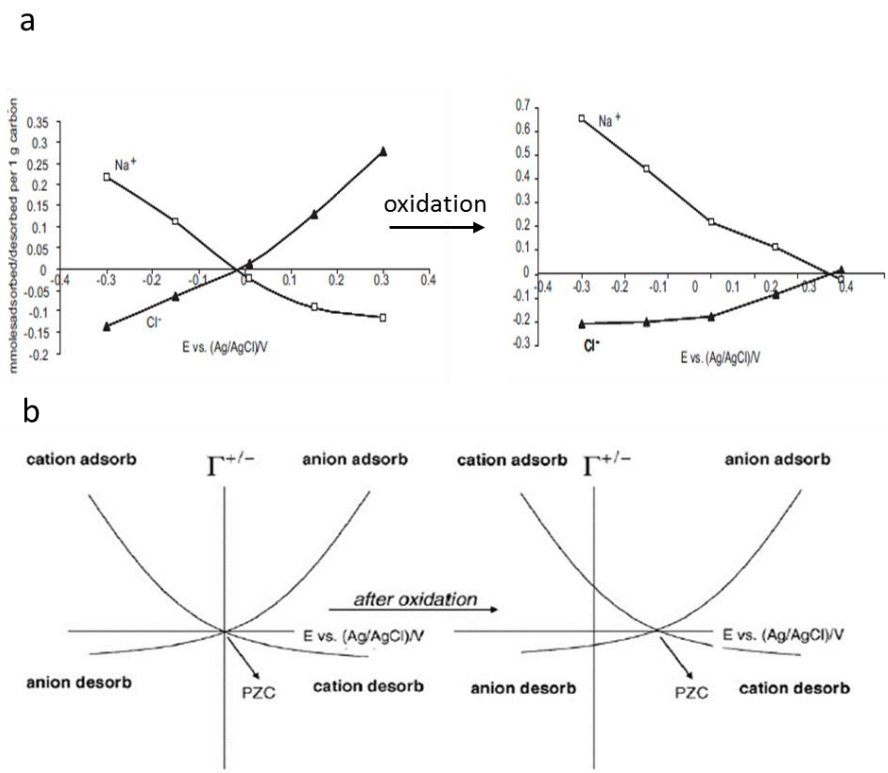

Figure 2-21. Adsorption and desorption characteristics of Na^+ (cation) and Cl^- (anion) ion per electrode unit mass according to E_{pzc} of surface oxidized carbon electrode (oxidation by HNO_3), (a) experimental data, (b) schematic based on experimental data [48].

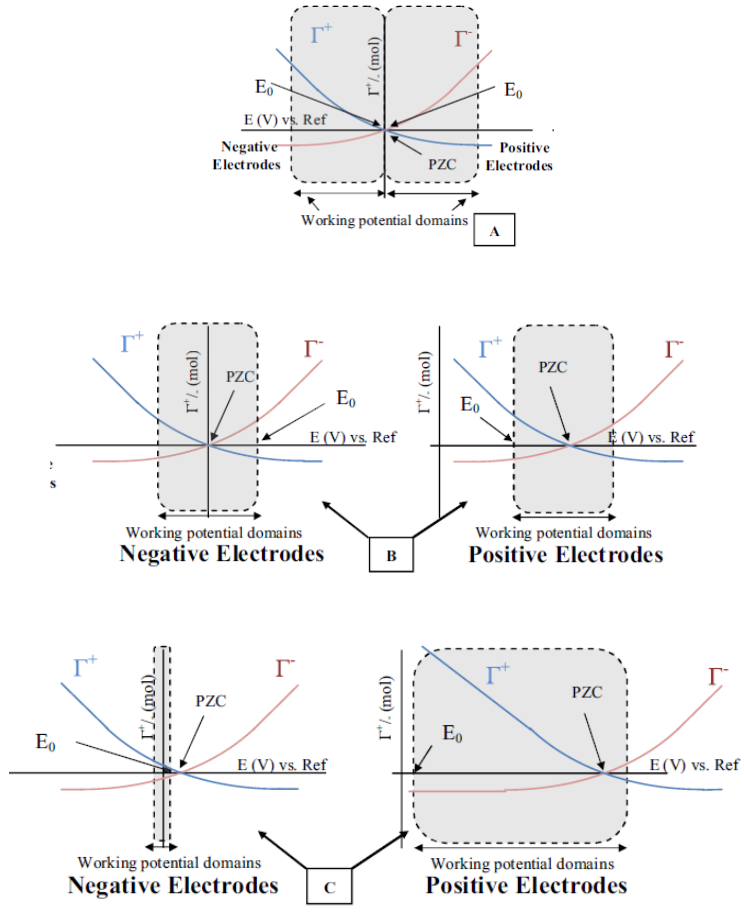

Figure 2-22. Relationship between ion adsorption capacity and changes of electrode properties (E_{pzc} and working potential) in long-term operation (a) initial state, (b) the state when the inversion point is reached, and (c) long-term operation state in which oxidation phenomenon intensifies [25].

3. The quantitative analysis of detailed Faradaic reaction and the effect of reaction products on deionization performance

3.1. Materials and Methods

3.1.1. Electrode fabrication

Following the previous studies [21, 49], carbon composite electrodes for CDI and MCDI processes were fabricated with a mixture of 86 wt% activated carbon (MSP20X, Kansai Coke and Chemicals, Japan), 7 wt% carbon black (super P, Timcal) and 7 wt% polytetrafluoroethylene (PTFE, Aldrich). Activated carbon and the carbon black were thoroughly mixed for one night and then it was pasted with PTFE and several drops of ethanol. The mixture was rolled to flat sheet carbon electrode by roll presser at 60℃ and 200 rpm. This fabricated carbon electrode (~300 μm of thickness) was dried overnight in vacuum oven at 120℃. BET surface area of the fabricated electrode was 1575 m^2/g.

3.1.2. Capacitive deionization experiments

CDI and MCDI systems were carried out a three electrode flow mode system cell (Figure 3-1) capable of investigating the capacitive deionization and the electrochemical performance of the electrodes. Two fabricated carbon electrodes were cut into round shape (20 mm in diameter with 3 mm center-hole in diameter) and put on each graphite sheet (current collector) connected by a cycler (WBSC3000, WonATech, Republic of Korea). In terms of MCDI system, cation exchange membrane and anion exchange membrane (CMX and AMX, Neosepta, ASTOM Co., Japan) were placed on cathode and anode respectively. A nylon spacer (25 mm diameter) was placed between the electrodes or the ion exchange membranes for water passage. As feed solution, 10 mM of sodium chloride solution was supplied at 2 ml/min of constant flow rate by peristatic pump. The constant potentials of 1.2 V were applied for 15 min of charging step, while discharging step was proceeded by short circuit (constant 0 V) for another 15 min. Effluent conductivity (3574-10C, HORIBA, Japan) and pH (9618-10D, HORIBA, Japan) were continuously measured and their measurements were utilized to calculate the salt adsorption capacity and efficiency. All deionization experiments were performed twice to investigate reproducibility and presented one selected result.

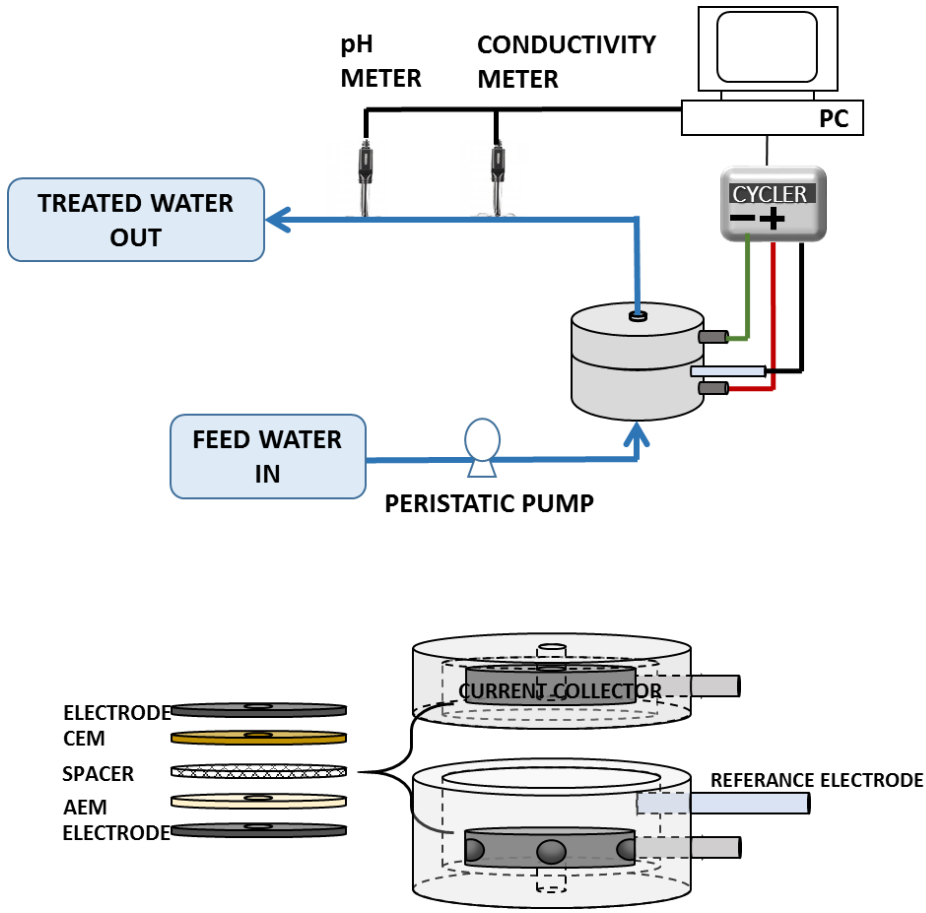

Figure 3-1**.** Scheme of the flow mode three electrode CDI and MCDI systems.

3.1.3. Removal of dissolved oxygen in feed

The N_2 gas purged feed was provided in the same manner as the CDI experiment to investigate the effect of oxygen. N_2 gas was purged from 2 hr before the experiment to the end of the experiment and DO was maintained at less than about 0.1 mg/L.

3.1.4. Electrochemical characterizations

GCD was performed in the same three electrode flow cell as the capacitive deionization experiment to measure cell voltage and working potential of the each electrode. The cell was charged and discharged within zero to 1.2 V at a constant current ($2.5 mA/cm^2$) with 10 mM NaCl feed solution. Working potential of anode and cathode was simultaenously mesured with Ag/AgCl (KCl sat'd) reference electrode.

3.1.5. Measurement of effluent H_2O_2

The concentration of hydrogen peroxide was determined with the 2,9-dimethyl-1,10-phenanthroline (DMP) method [50]. A 1 ml of the effluent was collected followed by mixing with 1 ml of DMP solution (1 g of neocuproine (Aldrich) dissolved in 100 mL of ethanol), 1 ml of 0.01 M copper (II) sulphate (Aldrich), and 7 ml of phosphate 0.1 M buffer solution. Then, the absorbance of the mixed solution was measured at 454 nm (Agilent Technologies, USA). The concentration of H_2O_2 was calculated with the following equation:

$$[H_2O_2] = (A_{sample} - A_{blank})/1500 \quad (3\text{-}1)$$

, where $[H_2O_2]$ is the concentration of the hydrogen peroxide (M); A_{sample} is the absorbance of the sample, and A_{blank} is the absorbance of the blank. The blank was taken from the effluent before the CDI experiment was started.

3.1.6. Measurement of surface pH of electrodes

For the surface pH measurements, a flat tip pH electrode was used (HANNA HI 1413B, HANNA instruments, USA) and the pH of opposite electrode surface (or ion exchange membrane) of the anode and the cathode was measured. The electrode surface pH was measured by decomposing the cell after applying 1.2 V for 5 min.

3.1.7. Deionization capacity evaluation

The deionization capacity of CDI and MCDI was evaluated with the salt adsorption capacity (SAC), which is the amount of removed ions per unit area of the electrode during the charging step. SAC was calculated by:

$$\text{SAC (mg/g)} = \frac{\int M_w \cdot ([NaCl]_{in} - [NaCl]_{out}) \cdot \Phi \cdot dt}{M_{electrode}} \quad (3\text{-}2)$$

where M_w is molecular weight of NaCl (58.44 mg mmol^{-1}); $[NaCl]_{in}$ and $[NaCl]_{out}$ are the influent and effluent concentration of NaCl (mmol L^{-1}); Φ is flow rate (L min^{-1}); $M_{electrode}$ is electrode weight(g).

[NaCl] were obtained from the measured conductivity values with pH compensation like Equation (3-3), assuming that other ions (e.g. bicarbonate) except Na^+, Cl^-, H^+, and OH^- exist negligible.

$$K' = K - FC_{H^+}u_{H^+} - FC_{OH^-}u_{OH^-} \quad (3\text{-}3)$$

(K' and K: pH compensated and measured effluent conductivity (S cm^{-1}), *F*: Faraday's constant (96,485 C mol^{-1}), C: ion concentration (mol cm^{-3}), u: ion mobility(cm^2 V^{-1} s^{-1}))

The initial third cycle (when the system was stabilized) was chosen for measuring deionization capacity.

3.1.8. Charge consumption distribution

The charge consumption in CDI and MCDI were assumed to be composed of adsorption, Faradaic reactions, co-ion repulsion, and charge leakages as shown in Equation (3-4).

$$C_{total} = C_{adsorption} + C_{Faradaic\ reaction} + C_{co-ion\ repulsion} + C_{leakage} \quad (3\text{-}4)$$

Following the previous reports [49], total charge (C_{total}) and adsorption charge ($C_{adsorption}$) were calculated as:

$$C_{total} = Q = \int I \cdot dt \quad (3\text{-}5)$$

$$C_{adsorption} = \int ([NaCl]_{in} - [NaCl]_{out}) \cdot \Phi \cdot dt \cdot F \quad (3\text{-}6)$$

, where I is current (A); F is Faraday's constant (96,485 C mol^{-1}); t is charging time.

Major Faradaic reactions are assumed to be the reaction for H_2O_2 (Reaction (3-12)) as reduction and the H^+ production reactions as oxidation. Thus, charge for Faradaic reaction ($C_{Faradaic\ reaction}$) was derived by:

$$C_{Faradaic\ reaction} = C_{reduction} + C_{oxidation} \approx C_{H_2O_2} + C_{H^+} \quad (3\text{-}7)$$

$$C_{H_2O_2} = \int 2 \cdot [H_2O_2]_{out} \cdot \Phi \cdot dt \cdot F \quad (3\text{-}8)$$

$$C_{H^+} = \int_{t1}^{t2} \left([H^+]_{out} - [H^+]_{peak\ pH}\right) \cdot \Phi \cdot dt \cdot F \quad (3\text{-}9)$$

where $[H_2O_2]_{out}$ is the effluent concentration of H_2O_2 (mol L^{-1}); $[H^+]_{out}$ is the effluent concentration of H^+ (mol L^{-1}); $[H^+]_{peak\ pH}$ is the H^+ concentration at peak pH (the highest pH during charge); t_1 is when the pH decrease started after the peak pH; t_2 is when the end of charge.

In Equation (3-8), the charge consumption for H_2O_2 production ($C_{H_2O_2}$) is obtained by converting the H_2O_2 concentration into the charge, following the stoichiometric ratio of Reaction (3-12).

Assuming that the oxidations occurring before the peak pH (Figure 3-2) in charging process are negligible, the charge consumption for H^+ production (C_{H^+}) is calculated from the concentration of H^+ that produced after the peak pH. In addition, the amount of generated H_2O_2 was constant (Figure 3-4) enough to maintain the peak pH. However, since the pH was decreased by the oxidation reactions (H^+ productions), the amount of produced H^+ was calculated considering the pH decreased with respect to the peak pH in Equation (3-9). Notably, the calculated charge for Faradaic reaction may be underestimated, especially for MCDI, because the actual surface reactions may not be fully reflected from the effluent pH and H_2O_2 due to the restricted transfer of reactants/products (H_2O_2, H^+, and OH^-).

The charge consumption for leakage was obtained from leakage current after adsorption saturation in MCDI. The leakage current (residual current - Faraday

reaction current) at saturation was assumed to be the same during the entire charging process and to flow in the same amount in the CDI system.

$$C_{leakage} = (I_{residue} - I_{Faradaic\ reaction})_{at\ saturation} \cdot t \quad (3\text{-}10)$$

The charge consumption for co-ion repulsion was calculated as:

$$C_{co-ion\ repulsion} = C_{total} - C_{adsorption} - C_{Faradaic\ reaction} - C_{leakage} \quad (3\text{-}11)$$

Each charge consumption rate (%) is calculated as a percentage of the consumed charge for the total charge (Q). For example, the adsorption charge rate (so called charge efficiency) is calculated as $\frac{C_{adsorption}}{C_{total}} \times 100$.

3.2. Results and Discussion

3.2.1. Temporal and spatial pH distribution

Figure 3-2 shows the effluent pH in CDI, N_2 purged CDI, and MCDI systems. As shown in the Figure, the effluent pH of both of CDI and MCDI systems during charging step tended to increase initially and then decrease after exceeding the peak pH. However, the effluent pH in the CDI and N_2 purged CDI processes fluctuated more severely from 10 to 4, while that in MCDI process was less only from 7 to 5. This type of pH fluctuation is similar to the previous reports that the effluent pH was initially increased and then decreased during the charging step [23, 24, 30]. This observation regarding pH fluctuation was explained by the difference in the adsorption rate between H^+ and OH^-, or side reactions [23]. Especially, Faradaic reaction such as oxygen reduction and carbon oxidation could explain the pH fluctuation that occurs during CDI operation. In addition, low pH fluctuations of MCDI have been previously described as less oxygen reduction by limited transport of oxygen through ion exchange membranes [13]. Also, the limited migration of other reaction products (H^+, OH^-) can affect the less effluent pH fluctuation. On the other hand, the reason why the pH fluctuation was similar to the CDI in the N_2 purged CDI with low DO is considered to be that there was a limit in controlling all the Faradaic reactions by only the DO blockage of the feed.

Figure 3-3 shows the different pH of electrode surface between anode and cathode in CDI, N_2 purged CDI, and MCDI systems during charging step. In the case of

CDI, the pH of the anode was 3.4 and the pH of the cathode was 11.1. However, MCDI showed greater pH difference than CDI, the pH of the anode was 1.5 and the pH of the cathode was close to 11.7. The ion exchange membranes covering the electrodes in MCDI were also severely separated into acidic (~2.0) at the anode and alkaline (~10.7) at the cathode. Interestingly, the change in effluent pH in MCDI was smaller, but the change in surface pH was greater than that of CDI. In N_2 purged CDI, the surface pH of cathode was 11.0, almost similar to CDI, and the anodic surface was 2.4, which was about the median of CDI and MCDI.

The simultaneous localized pH, which is acidic at the anode surface and basic at the cathode surface, can be attributed to the Faradaic reactions [33, 51, 52]. Plausible Faradaic reactions from Reaction (3-12) to (3-18) were suggested considering the measured working potential region (about -0.4 to 0.8 V vs. Ag/AgCl (KCl sat'd)) of CDI and MCDI with applied cell voltage of 1.2 V. Redox potential at bulk pH 7 was determined by Nernst' equation ($E = E^0 - 0.059 \bullet \text{pH}$).

$$O_2 + 2H^+ + 2e^- \leftrightarrow H_2O_2,\ E = 0.087\ \text{V (vs. Ag/AgCl (KCl sat'd))} \quad (3\text{-}12)$$

$$O_2 + 2H_2O + 4e^- \leftrightarrow 4OH^-,\ E = -0.210\ \text{V (vs. Ag/AgCl (KCl sat'd))} \quad (3\text{-}13)$$

$$H_2O_2 \leftrightarrow O_2 + 2H^+ + 2e^-,\ E = 0.087\ \text{V (vs. Ag/AgCl (KCl sat'd))} \quad (3\text{-}14)$$

$$C + H_2O \leftrightarrow C\text{–}O_{ad} + 2H^+ + 2e^-,\ E = -0.404\ \text{V (vs. Ag/AgCl (KCl sat'd))} \quad (3\text{-}15)$$

$$C + H_2O \leftrightarrow CO + 2H^+ + 2e^-,\ E = -0.093\ \text{V (vs. Ag/AgCl (KCl sat'd))} \quad (3\text{-}16)$$

$$C + 2H_2O \leftrightarrow CO_2 + 4H^+ + 4e^-,\ E = -0.404\ \text{V (vs. Ag/AgCl (KCl sat'd))} \quad (3\text{-}17)$$

$2H_2O \leftrightarrow O_2 + 4H^+ + 4e^-$, E = 0.617 V (vs. Ag/AgCl (KCl sat'd)) (3-18)

As shown the Reaction (3-12) to (3-18), cathodic reactions consume H^+ (Reaction (3-12) and (3-13)) [53], while anodic reactions produce H^+ (Reaction (3-14) to (3-18)) [27, 30]. However, note that some oxidations (Reaction (3-18)) cannot occur at low pH at the anode surface due to the increase in electrode reaction potential.

The greater changes of surface pH of MCDI are due to migration-limited reaction products (H^+ and OH^-) by ion exchange membranes. For example, H^+ was isolated from anion exchange membrane at the anode and OH^- was isolated from the cation exchange membrane at the cathode. Importantly, the highly maintained pH near the cathode in MCDI forms a condition in which an additional H^+ consumption reaction (reductions by Reaction (3-12) and (3-13)) is difficult. Likewise, the lower pH at the anode is not suitable for the H^+ production reaction (oxidations by Reaction (3-14) to (3-18)). In short, the additional Faradaic reaction cannot easily be developed in MCDI in comparison with CDI. Therefore, the limited migration of reactants and products such as O_2, H_2O_2, H^+, and OH^- severely changed the surface pH and the lack of reactants on the surfaces can reduce the further Faradaic reaction in MCDI system.

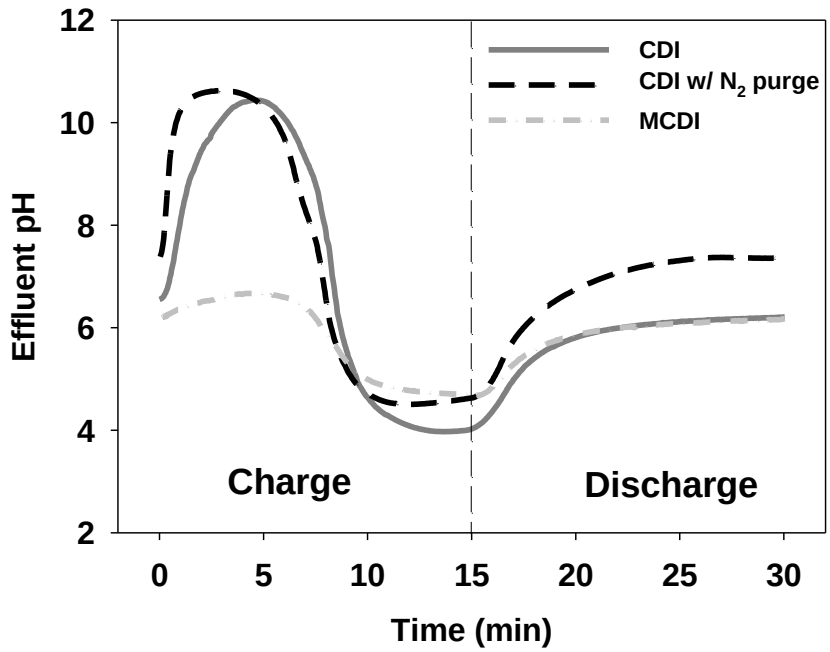

Figure 3-2. The effluent pH in CDI, N_2 purged CDI, and MCDI systems. Applied cell voltage was 1.2/0 V in charging/discharging step.

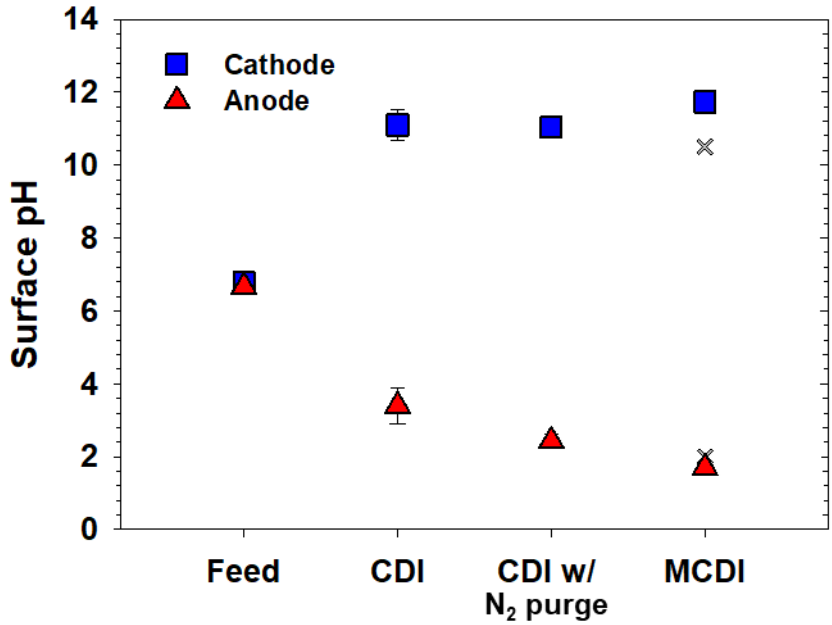

Figure 3-3. The measured surface pH of the electrodes and ion exchange membranes in CDI, N_2 purged CDI, and MCDI systems. In the MCDI system, x represents the surface pH of the ion exchange membranes (above: cation exchange membrane, below: anion exchange membrane). The electrode surface pH was measured by decomposing the cell after applying 1.2 V for 5 min. All measurements were repeated three times.

3.2.2. Hydrogen peroxide generation

Figure 3-4 shows the H_2O_2 concentration of effluent in CDI, N_2 purged CDI, and MCDI systems. The concentration of H_2O_2 in CDI was 37.0 μM, which is twice higher than that of CDI (~ 19.7 μM) and about 6.7 times higher than that of MCDI (~ 5.5 μM). The H_2O_2 concentration of all systems remained constant during the charging phase H_2O_2 generation occurs from the reduction of DO (Reaction (3-12)) and is thermodynamically feasible at an applied potential of 1.2 V, but the rate of reaction depends on the amount of DO. For example, the amount of DO in the N_2 purged feed was less than about 0.1 mg/L, and that in the no N_2 purged feed was about 6.0 mg/L. Therefore, the N_2 purged CDI and MCDI showed low H_2O_2 concentration because the oxygen reduction was suppressed by the decrease of the DO concentration by the oxygen removal or the decrease of the oxygen permeation through the membrane. However, the N_2 purged CDI still had a higher H_2O_2 concentration than MCDI despite the control of DO in feed. This means that due to the presence of oxygen contained in the carbon pores itself, only the DO blocking of the feed has a limitation in effectively controlling the generation of H_2O_2. In addition, the concentration of H_2O_2 in MCDI can be measured lower because the generated H_2O_2 was blocked to the effluent through the ion exchange membrane. Significantly, blocked H_2O_2 in MCDI can further limit anode oxidation due to the lower H_2O_2 concentration at the anode side. Thus, in the MCDI, where permeation of DO and H_2O_2 is difficult, the Faradaic reaction associated with H_2O_2 is limited.

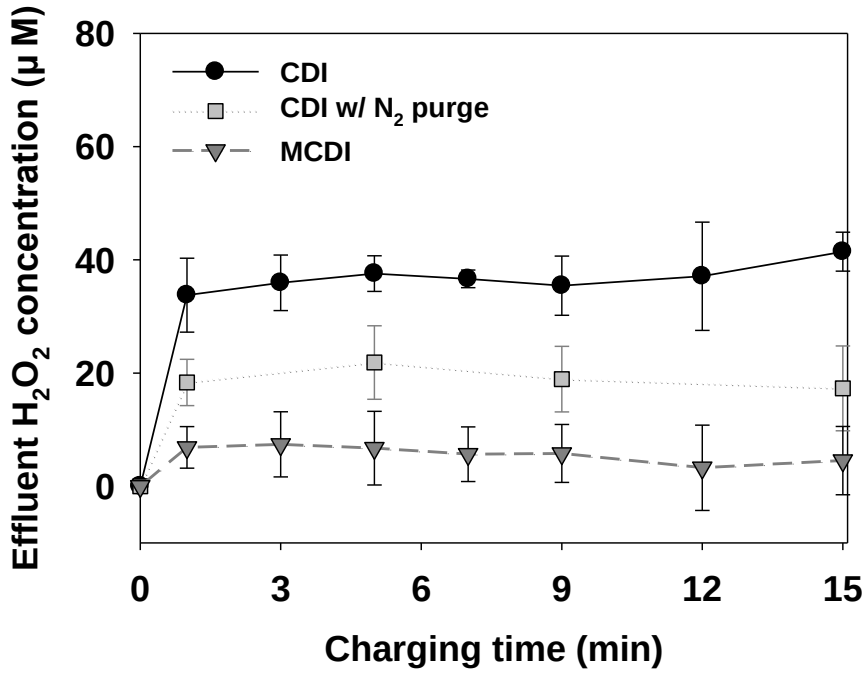

Figure 3-4. H_2O_2 concentration in the effluent of CDI, N_2 purged CDI, and MCDI at the applied cell voltage of 1.2 V.

3.2.3. Galvanostatic charge/discharge performance

Figure 3-5 shows the potential proflies of GCD of CDI (a) and MCDI (b) in the three electrode flow mode system at constant current of 2.5 mA/cm^2 in the range of zero to 1.2 V. In Figure 4, two important observations can be made.

First, the electrode applied potential of anode and cathode in CDI and MCDI systems was symmetrically distributed in 0.6 V when the cell voltage reached 1.2 V. The cathode had a working potential range of -0.4 to 0.2 V (vs. Ag/AgCl (KCl sat'd)) and the anode had a working potential range of 0.2 to 0.8 V (vs. Ag/AgCl (KCl sat'd)). The working potentials of the anode and cathode were also mesured applying constant voltage process (1.2 V charge and 0 V discharge) with an Ag/AgCl reference electrode and showed the same symmetrical potential distribution as the GCD results (Figure 3-6). As can be seen in Figure 3-7, the thermodynamically feasible Faradaic reaction can be determined from the working potential and surface pH of the electrode, and the Reaction (3-12) to (3-18) listed above belong to those reactions.

Next, the differnt extent of Faradaic reaction were observed from the linearity of the GCD potential profile in CDI and MCDI systems. MCDI had a more linear slope than CDI, indicating that more Faradaic reactions can occure in CDI system. This result is consistent with the results shown above, such as higher effluent H_2O_2 concentrations and more oxidation of long-term cycled anode in CDI. The MCDI result was also not a perfect straight line, but it has much better linearity as

opposed to CDI. In particular, the slope of the anode of MCDI was almost linear, which indicated that the oxidation hardly occured. Since the reduction products at the cathode (OH^-, H_2O_2) are restricted in migration to the anode by the ion exchange membrane, subsequent oxidation is difficult to develop in MCDI system.

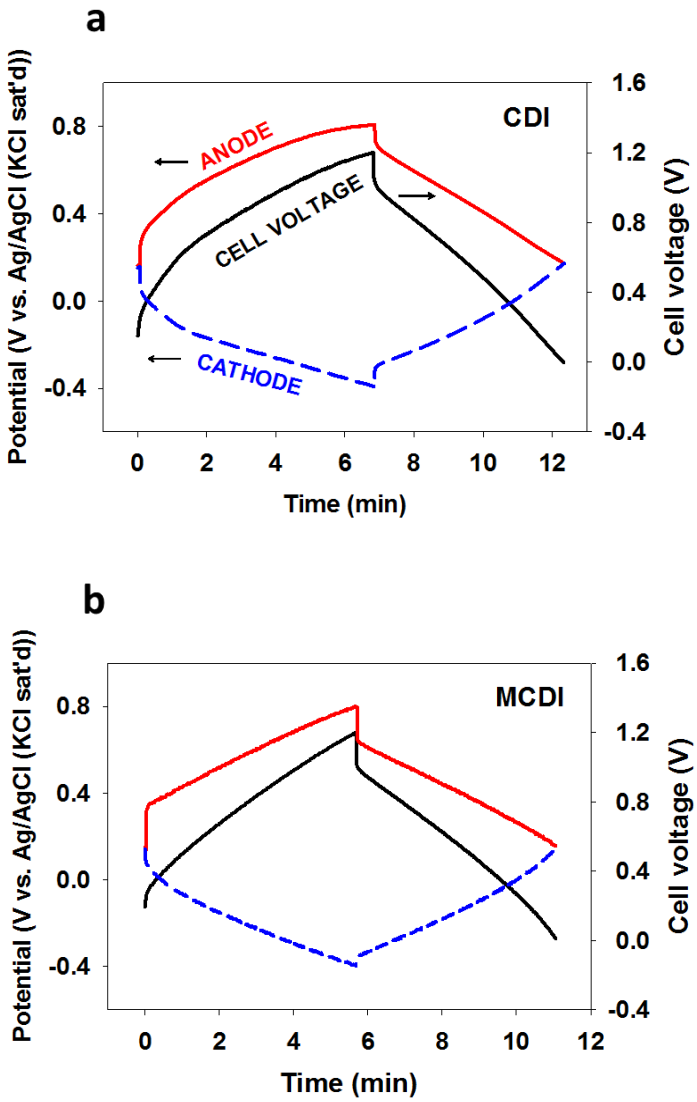

Figure 3-5. Galvanostatic charge/discharge in the three electrode flow mode (a) CDI and (b) MCDI systems with an Ag/AgCl (KCl sat'd) reference electrode, 10 mM NaCl, 2.5mA/cm^2 in the range of zero to 1.2 V

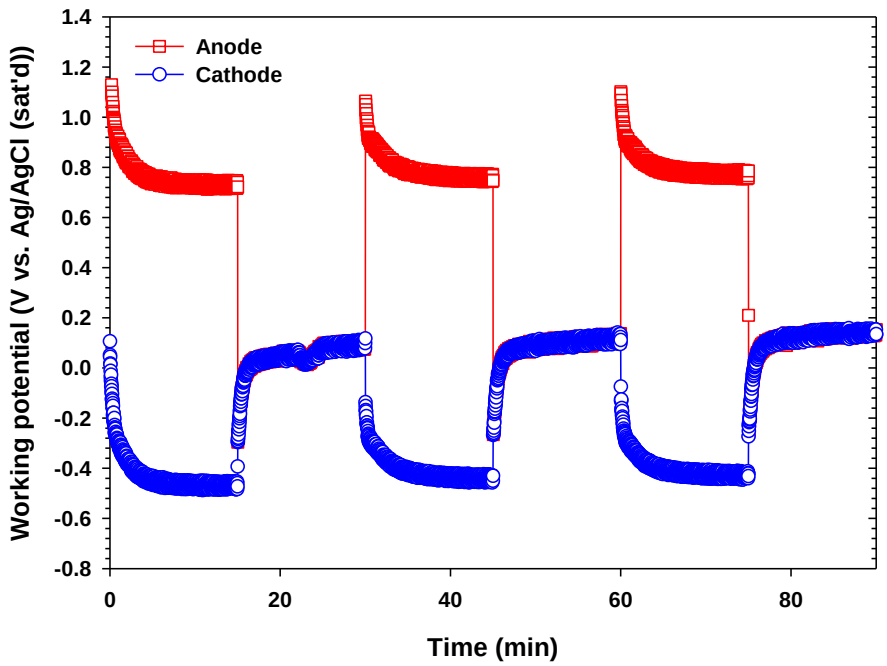

Figure 3-6. The working potentials of the anode and cathode mesured by applying CDI process (1.2/0 V of charge/discharge) in the three electrode flow mode CDI system with an Ag/AgCl (KCl sat'd) reference electrode.

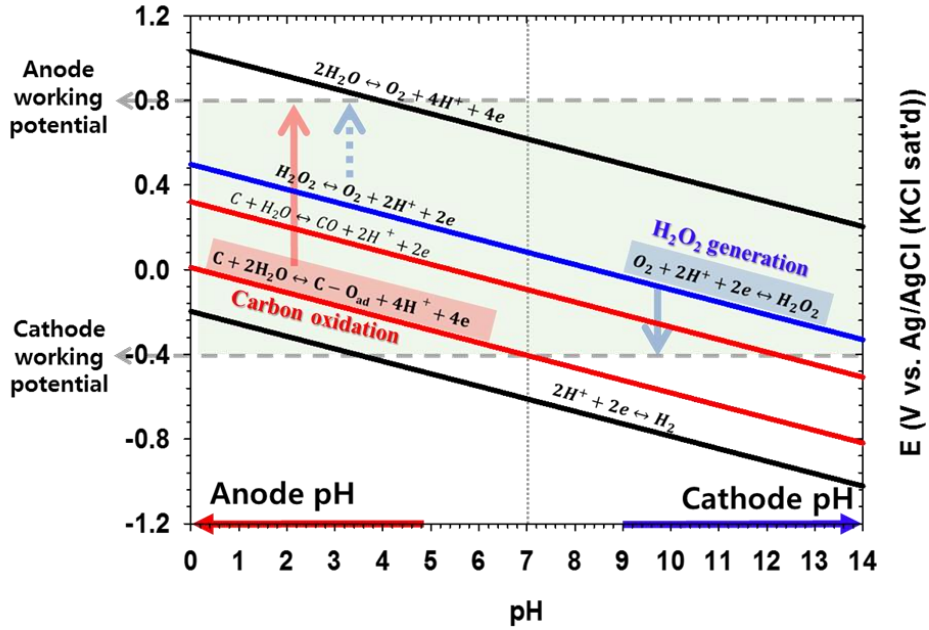

Figure 3-7. Determination of thermodynamically feasible Faradaic reactions at the function of the working potential and surface pH of the electrode in CDI and MCDI systems. The potentials of the reactions (E) were obtained by the Nernst' equation ($E = E^0 - 0.059 \bullet \text{pH}$).

3.2.4. Effect of Faradaic reaction products on deionization capacity

Figure 3-8 shows conductivity profiles and Figure 3-9 shows salt adsorption capacity (SAC) of CDI and MCDI systems. The decrease in conductivity during the charging process indicates the adsorption of ions to the electrodes, while the increase in conductivity during discharging indicates the release of ions from the electrodes. The decrease in conductivity (adsorption) at the charge step was greater in MCDI, which means that the adsorption of ions is better in MCDI. In a comparison of quantitative SAC, the SAC of MCDI was about 21.0 mg/g, which was about 1.2 times higher than that of CDI (15.3 mg/g). In general, the improved performance of MCDI has been reported to be due to reducing of co-ion repulsion [14, 15, 54]. However, here, an additional synergistic effect of Faradaic reaction and co-ion repulsion on adsorption capacity was considered. In CDI, the reaction products (H^+ from anode and OH^- from cathode) can act as co-ions that can increase the repulsion which is adverse to adsorption. On the other hand, in the MCDI, the OH^- at the cathode and the H^+ at the anode which are highly concentrated as co-ions can increase the charge potential inside the ion exchange membrane, and thus improve the storage of the counter ion. Therefore, as shown in Figure 3-10, the distribution of Faradaic reaction byproducts (distribution of pH) affect the desalination performance as increasing co-ion repulsion in CDI and as increasing internal co-ion charge potential inside of exchange membrane in MCDI.

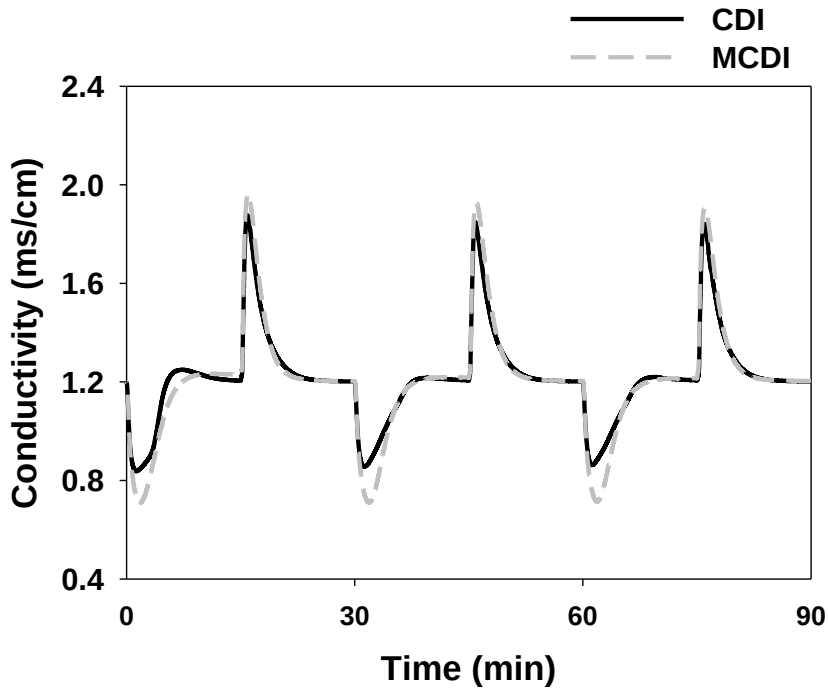

Figure 3-8. Conductivity profiles in CDI and MCDI systems at the first three cycles. Applied cell voltage was 1.2/0 V in charging/discharging step. All deionization experiments were performed twice to investigate reproducibility and presented one selected result.

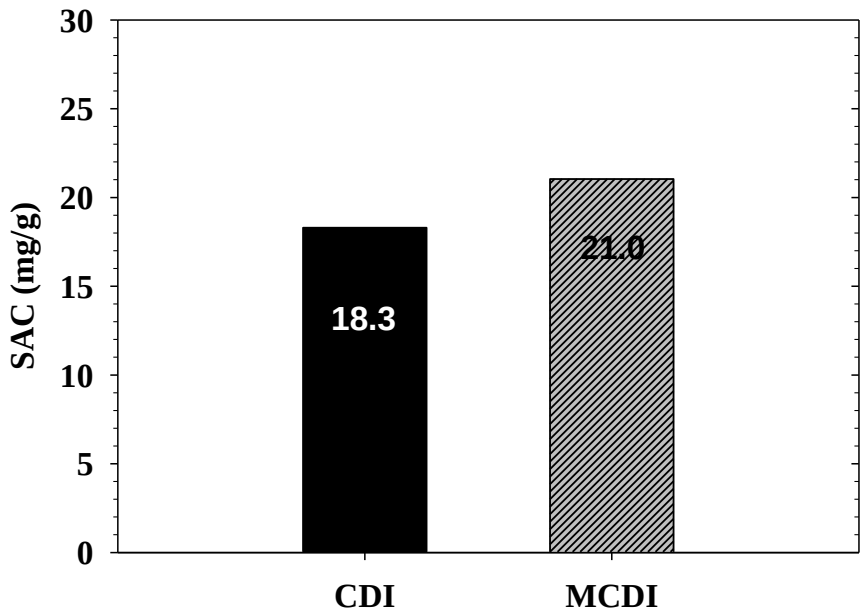

Figure 3-9. Salt adsorption capacity in the third charging process of CDI and MCDI systems**.** Applied cell voltage was 1.2/0 V in charging/discharging step. All deionization experiments were performed twice to investigate reproducibility and presented one selected result.

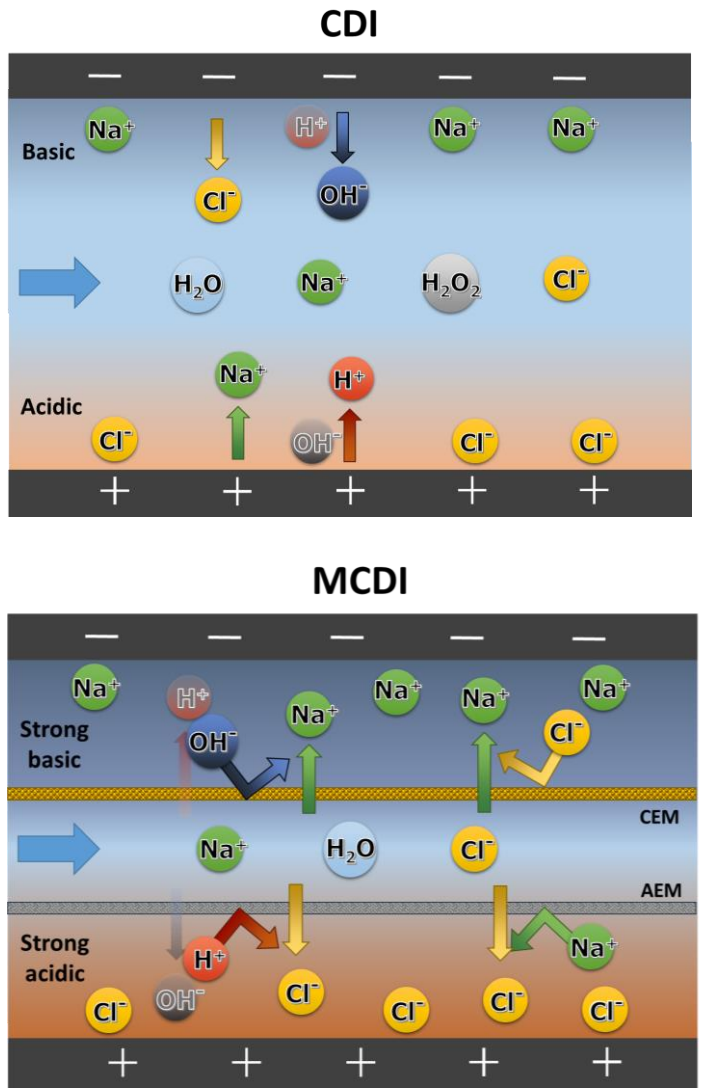

Figure 3-10. Schematic diagram of the effect of Faraday reaction products and co-ion repulsion on the ion adsorption performance during the charging process of CDI and MCDI systems.

3.2.5. Quantitative analysis of charge consumption distribution

Figure 3-11 shows the quantitative analysis of the charge consumption distribution consisted of adsorption, Faradaic reaction, co-ion repulsion and charge leakages in CDI and MCDI systems. Each charge consumption (%) was obtained according to the value shown in Table 3-1. The high deionization performance of the MCDI shown above could be achieved from the high charge efficiency of 92%. On the other hand, CDI consumed about 70% of the charge in deionization and the remaining 30% of the charge was consumed in the secondary area including Faradaic reaction and co-ion repulsion. With respect to the amount of charges consumed in the Faradaic reaction, about 1% of the charge was consumed in MCDI and about 10% in CDI, which is ten times that of MCDI. In the case of charge consumption for co-ion repulsion, it was about 13% in CDI assuming that there is no co-ion repulsion in MCDI. In the CDI system, the consumption of charge by Faradaic reaction was quantified for the first time and seemed not to be negligible since it is comparable to the charge that is consumed in co-ion repulsion. More importantly, the charges consumed in the Faradaic reaction are the charge consumed for the charge transfer reaction, but they can affect the charge for the co-ion repulsion. For example, the reaction products (H^+ and OH^-) generated by the Faradaic reaction increase the co-ion repulsion effect in CDI as working as co-ions, and can increase the charge consumed for co-ion repulsion. Therefore, in addition to the salt co-ion, the co-ions produced by Faradaic reaction can add co-ion repulsion charge in CDI system. Notably, the ratio of charges consumed in the

Faradaic reaction in one cycle may not be large (~10%), but the effect can be larger in prolonged cycle that change the surface properties little by little, which adversely affects the adsorption charge. On the other hands, in the MCDI system, charge efficiency was high because a very little charge was consumed in Faradaic reaction (~ 1%) and the co-ion repulsion was suppressed by the ion exchange membranes.

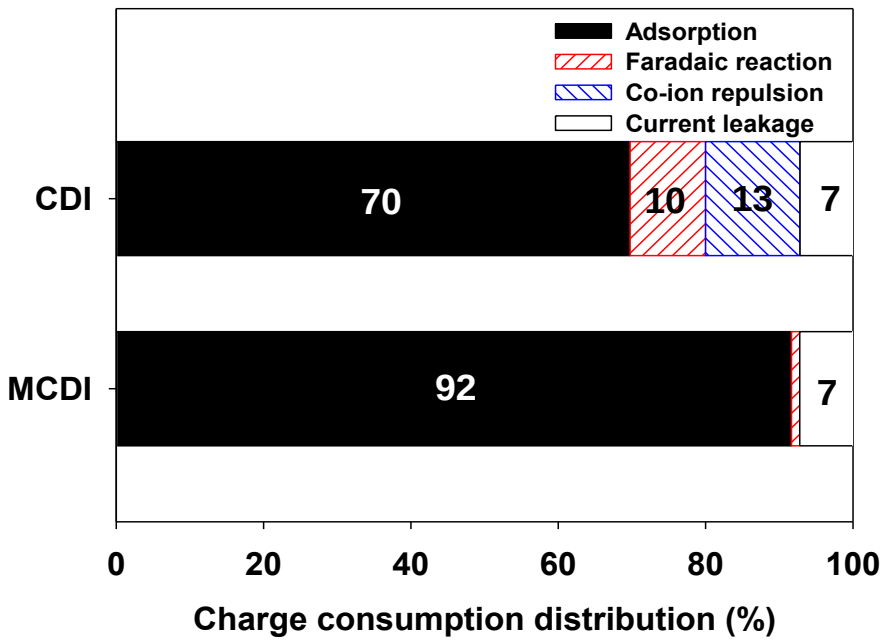

Figure 3-11. Charge consumption distribution of CDI and MCDI. The charge consists of adsorption, Faradaic reaction, co-ion repulsion, and current leakages. The charge consumed in the Faradaic reaction was obtained based on the concentration of Faradaic reaction byproducts.

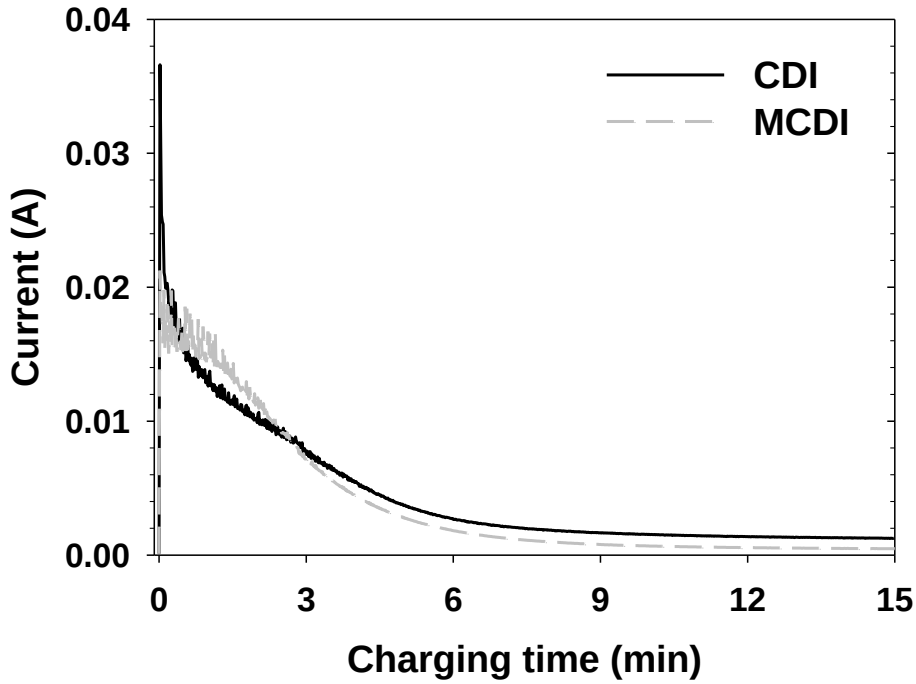

Figure 3-12. Current profile of CDI and MCDI systems in the charging step.

Table 3-1. Charge consumption distribution in CDI and MCDI.

(Coulomb)

	C_{total}	$C_{adsorption}$	$C_{H_2O_2}$	C_{H^+}	$C_{co-ion\ repulsion}$	$C_{leakage}$
CDI	**3.9**	**2.7**	**0.2**	**0.2**	**0.5**	**0.3**
MCDI	**3.6**	**3.3**	**0.0**	**0.0**	**0.0**	**0.3**

$$C_{total} = C_{adsorption} + C_{Faradaic\ reaction} + C_{co-ion\ repulsion} + C_{leakage}$$

$$C_{total} = \int I \cdot dt$$

$$C_{adsorption} = \int ([NaCl]_{in} - [NaCl]_{out}) \cdot \Phi \cdot dt \cdot F$$

$$C_{Faradaic\ reaction} = C_{reduction} + C_{oxidation} \approx C_{H_2O_2} + C_{H^+}$$

$$C_{H_2O_2} = \int 2 \cdot [H_2O_2]_{out} \cdot \Phi \cdot dt \cdot F$$

$$C_{H^+} = \int_{t1}^{t2} \left([H^+]_{out} - [H^+]_{peak\ pH}\right) \cdot \Phi \cdot dt \cdot F$$

$$C_{leakage} = (I_{residue} - I_{Faradaic\ reaction})_{at\ saturation} \cdot t$$

$$C_{co-ion\ repulsion} = C_{total} - C_{adsorption} - C_{Faradaic\ reaction} - C_{leakage}$$

$[H^+]_{peak\ pH}$ is the H^+ concentration at peak pH (the highest pH during charge); t_1 is when the pH decrease started after the peak pH; t_2 is when the end of charge; $C_{leakage}$ was obtained from leakage current at adsorption saturation based on MCDI.

3.3. Summary

In short term operation of CDI and MCDI systems, the characteristics of Faradaic reaction were analyzed and the effect of the Faradaic reaction on deionization capacity was interpreted. As evidence of Faradaic reaction, effluent and surface pH were changed and H_2O_2 was generated. Interestingly, the electrode surface pH was much more severely separated in MCDI despite the extreme fluctuations of effluent pH and highly generated H_2O_2 in CDI system. The pH of the anode surface was polarized to about 2, and the pH of the cathode surface was polarized to about 10. This is because the migration of reaction products (H^+, OH^-, H_2O_2) are restricted by the ion exchange membrane to the bulk or the surface of opposite electrode. The restricted transfer of reaction products can have two important effects. Firstly, further Faradaic reaction can be limited to develop due to the lack of reactants. Next, by increasing the electric charge potential (increase in co-ion products) inside the ion exchange membrane, it is advantageous to store the counter ions and improve salt adsorption capacity. More importantly, the charge consumption for Faradaic reaction and co-ion repulsion was quantitatively calculated for the first time. In CDI, Faradaic charge was initially 10% and the co-ion repulsion charge was 13%. Charge consumption by the Faradaic reaction was about 10% in the CDI system and about 1% in the MCDI system. The charge of the co-ion repulsion, which is known to reduce the performance of the CDI, was about

13%. Therefore, both Faradaic reaction and co-ion repulsion waste quite a lot of charge and decrease the deionization performance.

4. The analysis of changes in Faradaic reaction and deionization performance in long-term operation

4.1. Materials and Methods

4.1.1. Long-term capacitive deionization experiment

CDI and MCDI systems were carried out a three electrode flow mode system cell capable of investigating the capacitive deionization and the electrochemical performance of the electrodes. Used electrode and the deionization experiment was carried out the same way with short-term capacitive deionization experiment in part 3.1.1. and 3.1.2. 100 cycles of charging and discharging were repeated for long-term operation (3,000 min). The N_2 gas purged feed was provided in the same manner as the long-term CDI experiment. N_2 gas was purged from 5 hr before the experiment to the end of the experiment and DO was maintained at less than about 0.1 mg/L. All deionization experiments were performed twice to investigate reproducibility and presented one selected result.

4.1.2. Electrochemical characterizations of long-term cycled electrode

The potential of zero charge (E_{pzc}) of the long-term cycled carbon electrode including the pristine carbon electrode were analyzed by cyclic voltammetry (CV). CV was carried out in a three electrode batch mode cell and the electrode was cut into 18 mm rounds before the CV analysis. Ag/AgCl (KCl sat'd) and the pristine carbon electrode were used as a reference electrode and counter electrode, respectively. 100 mM NaCl was filled as an electrolyte and the scan rate was adjusted with a potentiostat (PARSTAT 2273, Princeton Applied Research,USA) at 1 mV/s. The potential range of the working electrode (-0.4 to 0.8 V) in CV was determined based on the galvanostatic charge/discharge (GCD) results.

Surface characterization of the pristine and the long-term cycled carbon electrode were investigated by Fourier transform infrared (FT-IR; Jasco Model FT-IR 200, Agilent, USA), X-ray photoelectron spectroscopy (XPS; Sigma Probe, ThermoVG, UK), BET-Surface area analyzer (BET; Micromeritics ASAP 2000, Micromeritics, USA), and scanning electron microscopy (SEM; JSM-6701F, JEOL, Japan). Before those measurement, the long-term cycled electrodes were thoroughly rinsed and dried. The wavenumber range for FT-IR measurement was 2,000-800 cm^{-1}. XPS spectra were obtained from the intensity of the carbon and oxygen atom. Nitrogen adsorptive was used at 77 K for BET measurement.

4.1.3. Evaluation of long-term cycled CDI performance

The long-term performance of CDI and MCDI was evaluated with the normalized SAC and charge consumption in comparison with short-term performance. The initial third cycle in the short term operation (when the system was stabilized) and the final cycle in the 100 cycled operation (after 3,000 min) were chosen for the performance evaluation. Normalized SAC (S/S_0) was obtained by dividing SAC (S) by the initial third SAC (S_0). The charge consumption distribution in long-term operation was obtained in the same way as short-term operation.

4.1.4. Modification of operating condition and electrodes

Modification of the electrode and operating condition were used to improve the stability of long-term operation. The modification of operating condition was performed with ab alternate reverse potential. All other operating conditions were the same, but in the charging process, both positive and negative potential were applied alternately. The charging process was carried out at 1.2 V and -1.2 V alternatively. The discharging process consisted of the same 0 V (short circuit). Figure 4-1 shows the cell voltage applied to the alternate reverse potentials.

The modification of electrodes was performed with an ion exchange polymer (IEP) coating. Used cation exchange polymer was sulfonated polyphenylene oxide (PPO) and the anion exchange polymer was PPO with quaternary ammonium (SIONTECH, Republic of Korea). The IEP was spin-coated with several drops on the electrode or steel surface. The thickness of coating layer was the same at about 30 μm. The polymer coated on the steel was immersed in deionized water and separated smoothly. The separated polymer film was covered on electrode and used as the IEP covered electrode. On the other hand, the electrode coated directly with the IEP was used as the IEP coated electrode.

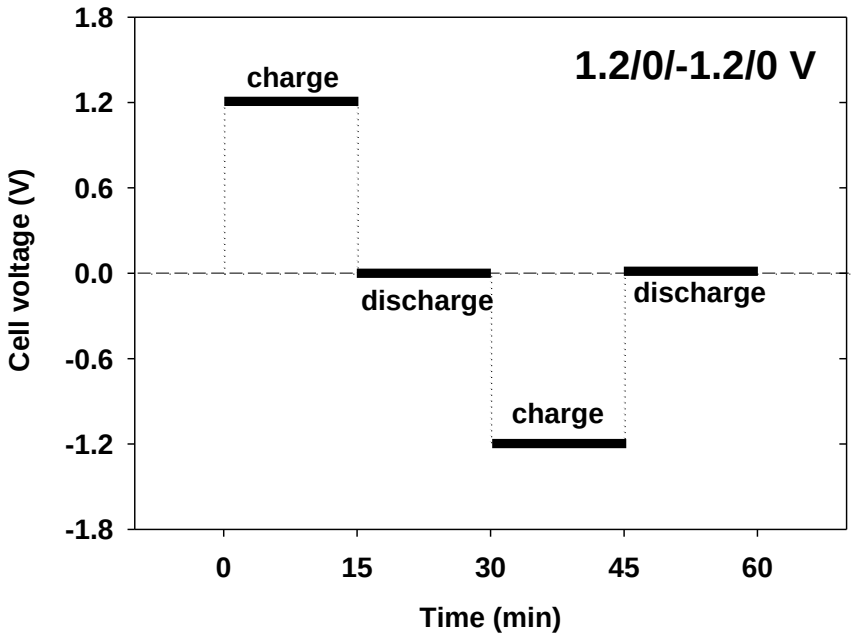

Figure 4-1. Cell voltage applied to the alternate reverse potentials.

4.2. Results and Discussion

4.2.1. Changes of Faradaic reaction in long-term CDI

To investigate the changes in characteristics of Faradaic reaction during long-term operation, the effluent pH and H_2O_2 concentration were measured in long-term CDI, N_2 purged CDI and MCDI systems. As shown in Figure 4-2, the effluent concentration of H_2O_2 was similar to the initial level and remained constant even in long term operation. It has been reported in our previous study that H_2O_2 is continuously generated in long-term operation of CDI [53]. Also, the same amount of H_2O_2 generated in MCDI and N_2 purged CDI in the short-term operation steadily occurred in the long-term operation. Next, as can be seen in Figure 4-3, fluctuations in effluent pH, especially acidification of the effluent, were observed in long-term operation similar to short-term operation. Acidification of the effluent means that the oxidation to produce H^+ occurs steadily in long-term operation. However, unlike MCDI and N_2 purged CDI, where pH fluctuations were almost similar, the peak pH in CDI was reduced from 11 (at 3^{rd} cycle) to 8 (at 100^{th} cycle) in CDI system. Considering H_2O_2, which is continuously produced in the same amount in long-term operation, the peak pH was also expected to remain at the same level (around pH 10), but not so. This change in peak pH can be attributed to the change in Faraday reaction during long-term operation and can be explained by the change in the working potential of the electrode.

As shown in Figure 4-4, the working potentials of the electrodes measured using Ag/AgCl (KCl sat'd) reference electrode in three electrode flow mode CDI (a) and MCDI (b) systems. The potential distributions of anode and cathode were symmetrical about 0.6 V initially in both systems. However, MCDI maintained symmetrical potential distribution well in long-term operation, while it changed asymmetrically in CDI system. In CDI, the working potential of the both electrodes positively shifted, but more potential was loaded to anode in the last three cycle. Thus, the potential distribution of the anode was about 0.7 V (0.2 to 0.9 V vs. Ag/AgCl) and the cathode was about 0.5 V (-0.3 to 0.2 V vs. Ag/AgCl), which showed asymmetric distribution. Similar results have been reported in previous studies that asymmetrically more potentials were falling on the anode [24, 29, 55]. On the other hand, in the MCDI system, there was a partial shift of the electrode working potential, but the symmetrical potential distribution was maintained. As shown in Figure 4-5, when the working potentials of anode more positively shifted, a thermodynamically feasible oxidation reaction such as oxygen generateion (Reaction 3-18) can be added.

$$2H_2O \leftrightarrow O_2 + 4H^+ + 4e^-,\ E = 0.617\ \text{V (vs. Ag/AgCl (KCl sat'd))} \qquad (3\text{-}18)$$

The development of additional oxidation may cause the effluent peak pH to decrease (Figure 4-3). However, further studies on the development of additional oxidation reactions is needed to precisely understand the changes of the Faradaic reactions in long-term operation.

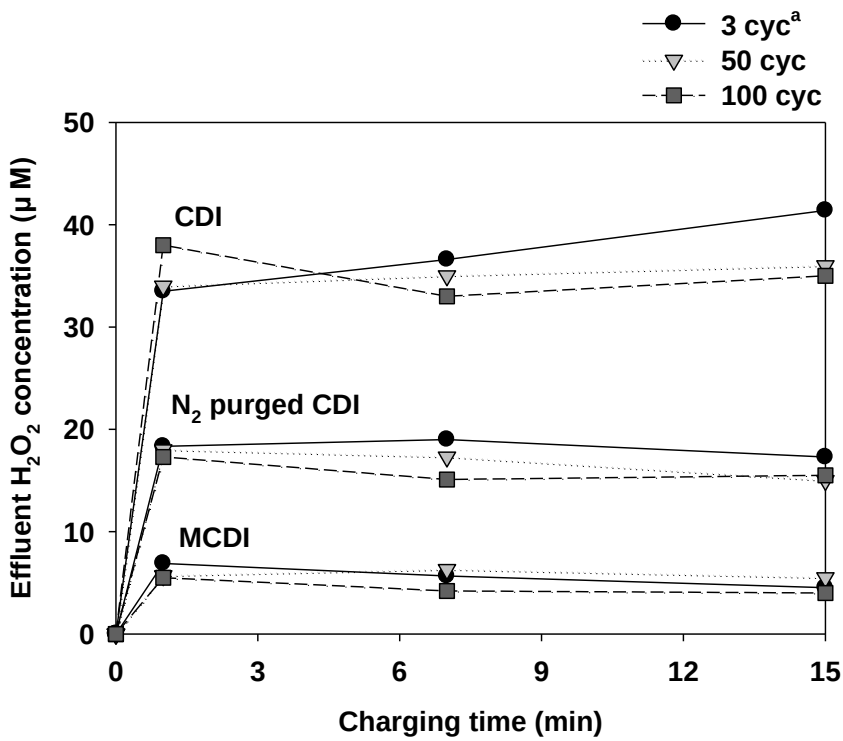

Figure 4-2. Changes of the effluent H_2O_2 concentration in long-term cycled CDI, N_2 purged CDI, and MCDI processes. The cell voltage of 1.2 V was applied in charging step. Results of 3 cyc[a] from Figure 3-3.

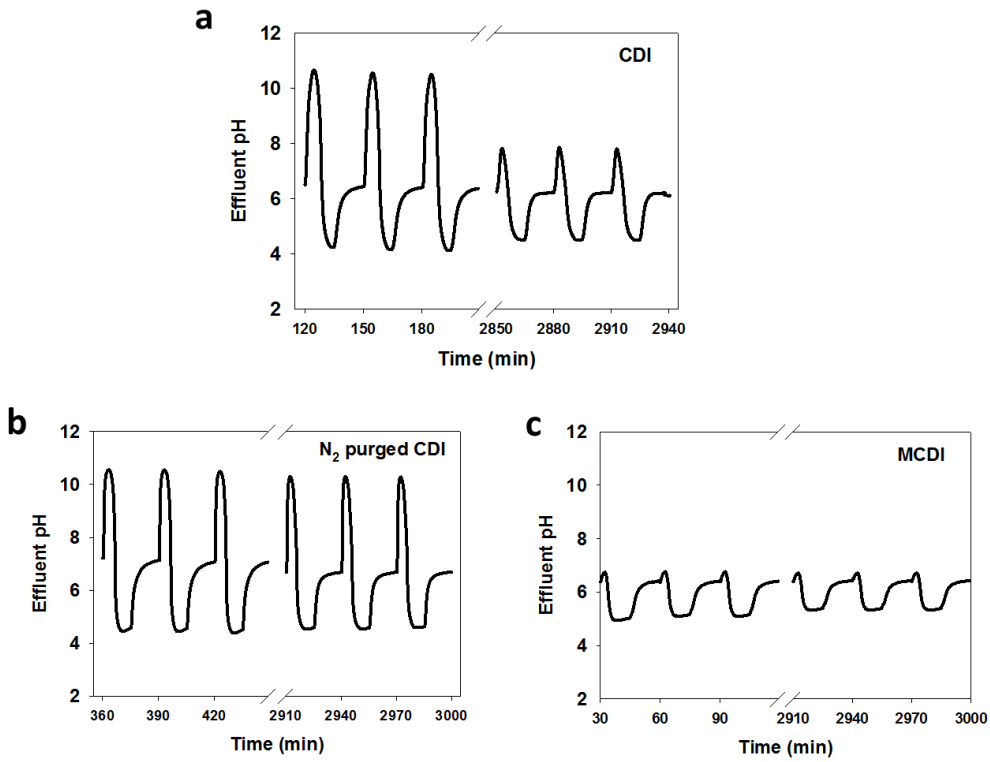

Figure 4-3. Changes of the effluent pH in long-term cycled (a) CDI, (b) N_2 purged CDI, and (c) MCDI processes. Applied cell voltage was 1.2/0 V in charging/discharging step.

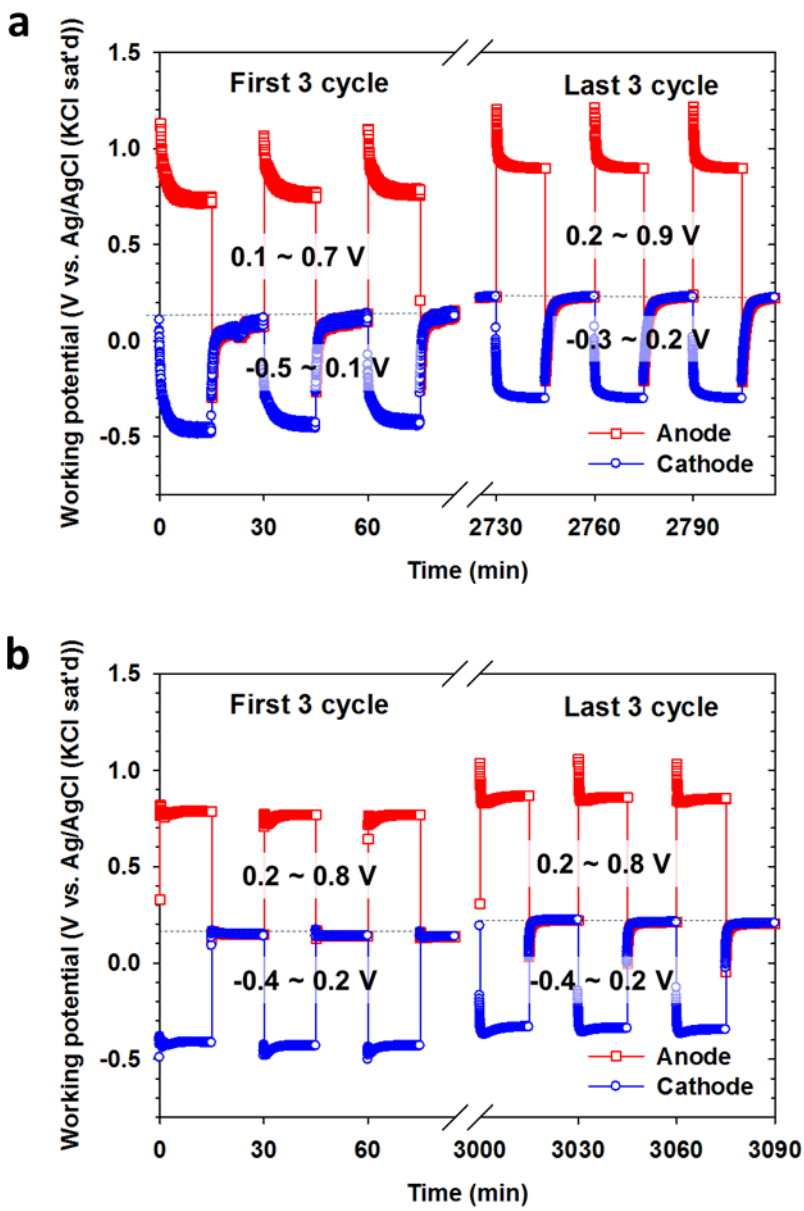

Figure 4-4. The change of working potential of anode and cathode in long-term (a) CDI and (b) MCDI systems. Applied cell voltage was 1.2/0 V in charging/discharging step.

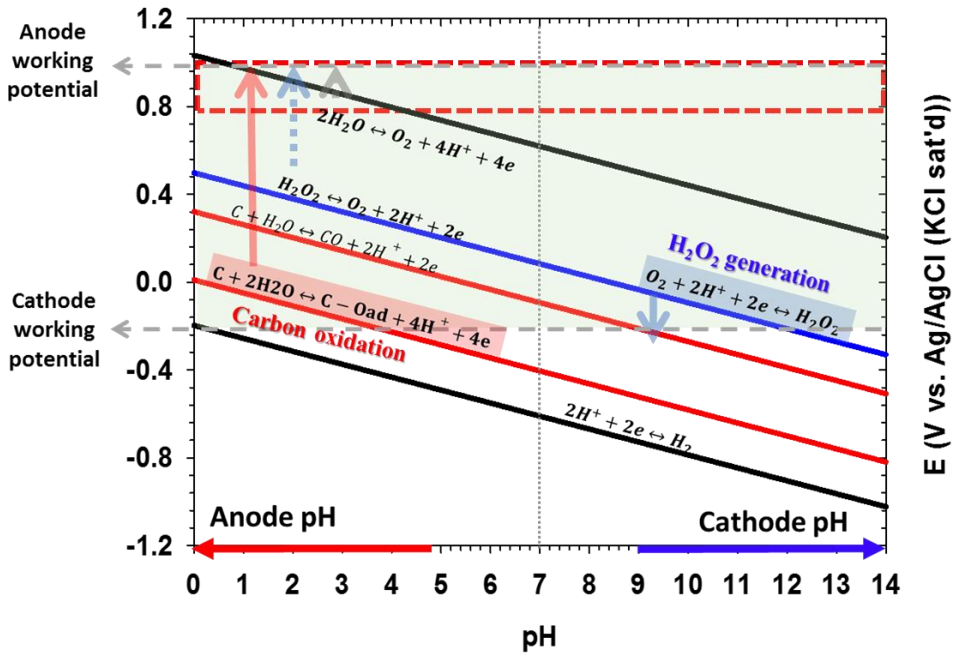

Figure 4-5. Asymmetrical change of the working potential of anode and cathode in long-term CDI experiment. Applied cell voltage was 1.2/0 V in charging/discharging step.

4.2.2. Asymmetric oxidation of anode

Figure 4-6 shows the FT-IR spectra of the long-term cycled anode and cathode in CDI and MCDI systems. The FT-IR results showed that some functional groups were newly found in long-term cycled anode and cathode in CDI and MCDI systems in contrast to the pristine electrode. In particular, in long-term cycled anode of CDI, peaks at wavelengths of about 1720, 1220, and 1150 cm^{-1} were highly developed. This bands respectively associated with oxygen-containing carbonyl and carboxyl groups (C=O, COOH) [56], C-O [57] and C-OH bond, which can closely related to in surface negative charge. COOH forms COO- from hydrolysis, leading to negative charge on the surface [46]. Conjugated C=C stretch structure were also found in most of long-term cycled electrodes at a wavelength around 1660-1500 cm^{-1}, but the change was little at the cathodes in both systems.

Figure 4-7 shows the CV of the long-term cycled anode and cathode in CDI and MCDI systems. From the CV profile, the potential of zero charge (E_{pzc}) of electrode at the minimum current was observed, which was significantly changed at the anode of long-term cycled CDI. During 100 cycles, the anode E_{pzc} of CDI was increased by about + 0.3 V, and the anode E_{pzc} of MCDI was about + 0.1 V and the cathode was almost unchanged. Positive shift of E_{pzc} in long-term cycled anode was similarly reported in the previous studies [13, 29]. Consistent with the changes of FT-IR spectra, the long-term cycled anode showed the largest change in E_{pzc}. In addition, the greatest increase in oxygen atomic content and noticeable reduction in the specific surface area were found in long-term cycled anode of CDI

by XPS spectra (Table 4-1) and BET analysis (Table 4-2). The degradation of carbon by carbon oxidation can decompose the pore structures. Unlike the change in the electrochemical performance of the anode electrode, no visible physical change was found by the SEM image (Figure 4-8). Thus, the oxidation reactions at anode can gradually change surface properties such as functional groups, E_{pzc}, oxygen atomic content and specific surface area, which can affect the long-term deionization performance.

$$H_2O_2 \leftrightarrow O_2 + 2H^+ + 2e^-,\ E = 0.087\ \text{V (vs. Ag/AgCl (KCl sat'd))} \quad (3\text{-}14)$$

$$C + H_2O \leftrightarrow C\text{–}O_{ad} + 2H^+ + 2e^-,\ E = -0.404\ \text{V (vs. Ag/AgCl (KCl sat'd))} \quad (3\text{-}15)$$

$$C + H_2O \leftrightarrow CO + 2H^+ + 2e^-,\ E = -0.093\ \text{V (vs. Ag/AgCl (KCl sat'd))} \quad (3\text{-}16)$$

$$C + 2H_2O \leftrightarrow CO_2 + 4H^+ + 4e^-,\ E = -0.404\ \text{V (vs. Ag/AgCl (KCl sat'd))} \quad (3\text{-}17)$$

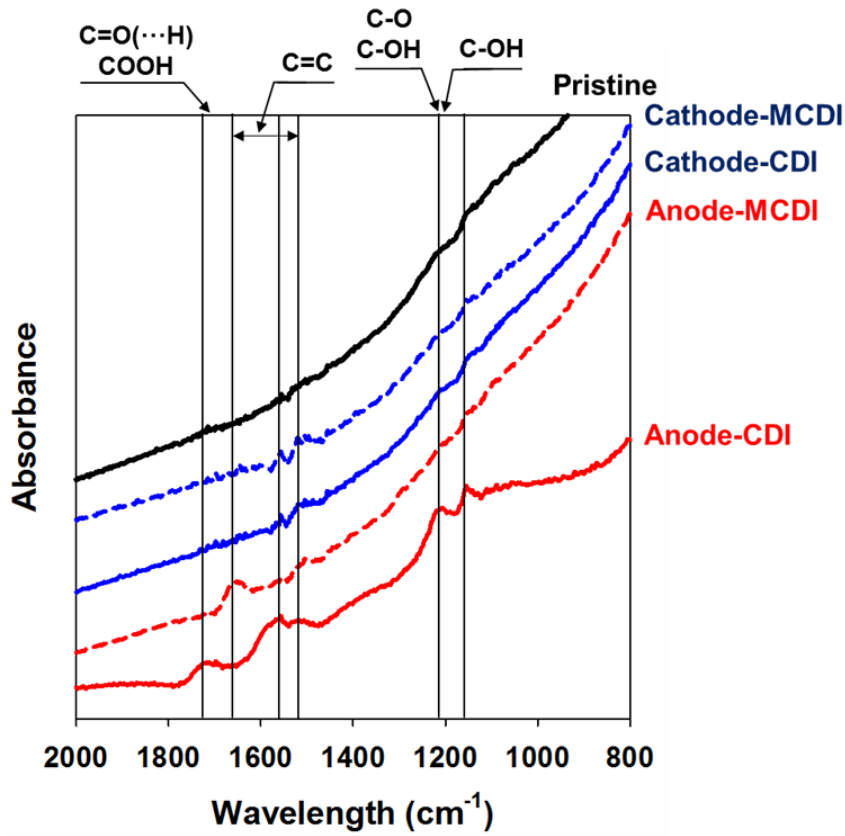

Figure 4-6. FT-IR spectra of the long-term cycled anode and cathode in CDI and MCDI systems. For long-term cycle, the charge/discharge cell voltage of 1.2/0 V was applied 100 times for 50 hr.

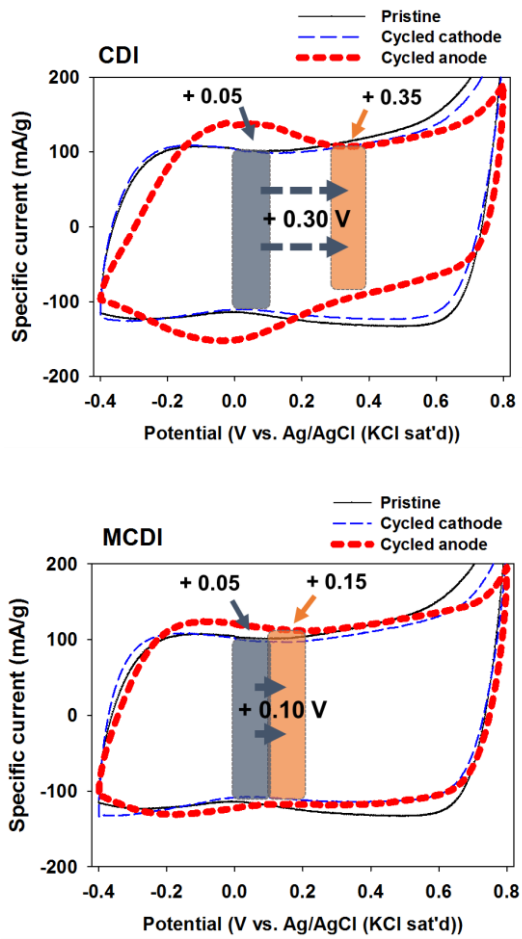

Figure 4-7. Cyclic voltammetry of the long-term cycled anode and cathode in CDI and MCDI systems. For long-term cycle, the charge/discharge cell voltage of 1.2/0 V was applied 100 times for 50 hr. Scan rate: 1 mV/s, electrolyte: 100 mM NaCl.

Table 4-1. Atomic content (%) of the long-term cycled anode and cathode in CDI and MCDI systems by XPS spectra in comparison with the pristine.

	Pristine	CDI_anode	CDI_cathode	MCDI_anode	MCDI_cathode
C1s	94.8	81.3	85.1	89.8	91.7
O1s	5.2	18.7	14.9	10.3	8.3

Table 4-2. BET surface area (m^2/g) of the long-term cycled anode and cathode in CDI and MCDI systems in comparison with the pristine.

(±30 m^2/g)

	Pristine	CDI_anode	CDI_cathode	MCDI_anode	MCDI_cathode
BET surface area (m^2/g)	**1575**	**1057**	**1537**	**1590**	**1677**

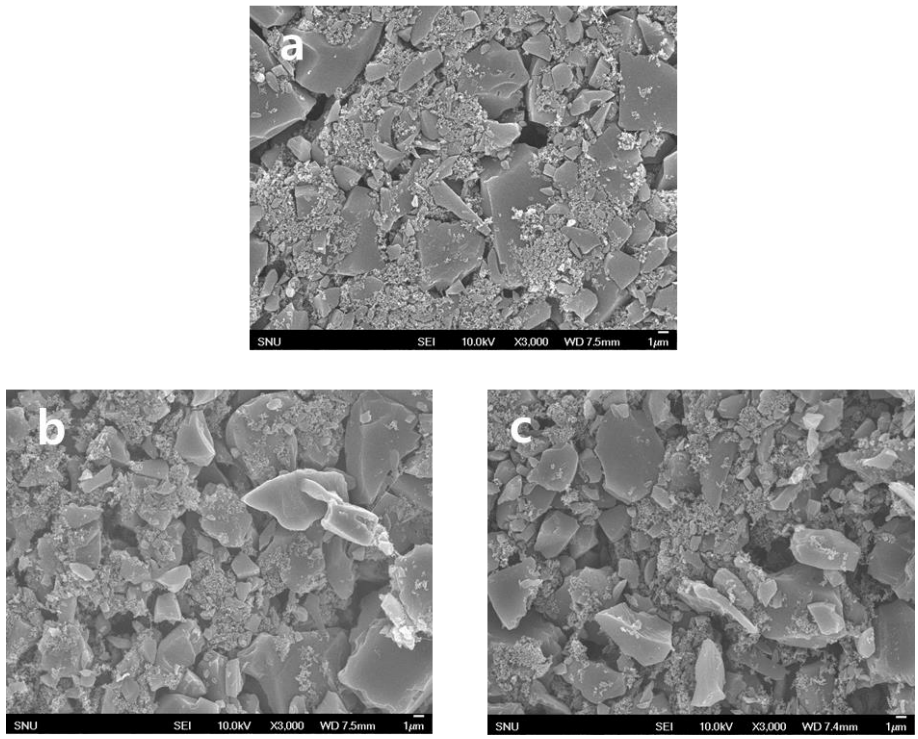

Figure 4-8. SEM images of (a) the pristine electrode, (b) long term cycled anode in CDI and (c) long term cycled anode in MCDI systems

4.2.3. Deterioration of long term performance

Figure 4-9 shows a conductivity profiles at the first three cycles and the last three cycles in CDI, N_2 purged CDI, and MCDI systems. The long term cycled CDI and N_2 purged CDI systems showed a significant change in the conductivity profile while the MCDI showed little change. The conductivity decrease (adsorption) and increase (desorption) peaks of CDI and N_2 purged CDI systems were remarkably reduced and the inversion region was shown in the last three cycles, in which the conductivity increased (desorption) during the adsorption step. Previous reports have observed the inversion region in CDI, which was explained by the oxidation of the anode. For example, the negative charge developed on anode surface in long term adsorbed cation during discharging and desorbed it during charging step [24, 29]. On the other hands, in MCDI, although surfaces of anode were partially oxidized during the long-term cycle in MCDI, the inversion effect can be prevented because co-ion adsorption is difficult by the ion exchange membrane.

Figure 4-10 shows normalized salt adsorption capacity (SAC) in the long-term CDI, N_2 purged CDI, and MCDI operations (a) and SAC at the initial and the last step in CDI and MCDI systems (b). The normalized SAC in the long-term showed a significant decrease of about 85% in the CDI and a decrease of about 20% in the MCDI compared to the initial SAC (S_0). The long-term SAC of N_2 purged CDI decreased slightly less (67%) than that of CDI, but it did not reach the performance of MCDI. In the last cycle, the absolute difference between the two values reached about 560% (2.7 mg/g for CDI and 17.9 mg/g for MCDI). The SAC of MCDI was

initially higher than CDI (~ 17% high) and was more beneficial in the long term (~ 560%). The relatively stable SAC in long-term MCDI operation was reported and interpreted as a result of less electrode oxidation due to low oxygen permeability by ion exchange membranes [13]. Furthermore, the generated H_2O_2, H^+, and OH^- in addition to DO can also be restricted by ion exchange membranes, which can effectively prevent additional Faradaic reactions. For example, removal of only DO by N_2 purging of feed maintained a higher efficiency than atmospheric condition, but still had more performance degradation than MCDI system where DO and other reaction byproducts (H^+, OH^-, H_2O_2, etc.) were controlled together. Therefore, the MCDI system was more effective for long-term stability by preventing the surface reactions that causes the oxidation of the electrode. On the other hand, the deterioration of CDI performance is likely to occur due to the stronger Faradaic reaction, especially oxidation of the anode. Carbon oxidation at the anode changed the surface charge of the electrode to negative during the long-term operation and resulted in asymmetric distribution of the working potential (Figure 4-4a). As a result, during the discharge process, some cations are adsorbed on the surface of the anode having a negative charge, and on the other hand, desorption phenomenon occurs in which the adsorbed ions are pushed out during the charging process as shown in Figure 4-11. Thus, the inversion region was observed found (Figure 4-9) and SAC was greatly reduced in CDI.

In fact, the anode of MCDI seemed to be also partially oxidized after long-term operation from the surface analysis result of FTIR, CV, and XPS data. However,

although the MCDI anode had a change of about one third of the E_{PZC} shift compared to the CDI anode, the performance decline in long-term operation was much less (~17% decrease). This may be due to the fact that the MCDI has little effect on the co-ion repulsion by the ion exchange membrane. As shown in Figure 4-12, since the oxidized anode is covered with an anion exchange membrane, the cation cannot be adsorbed to the anode having a partial negative charge at the discharging step, and the repulsion effect is not improved even at the charging stage. Therefore, the ion adsorption capacity of MCDI with a membrane may not be significantly affected by changes of E_{pzc} of the electrode surface.

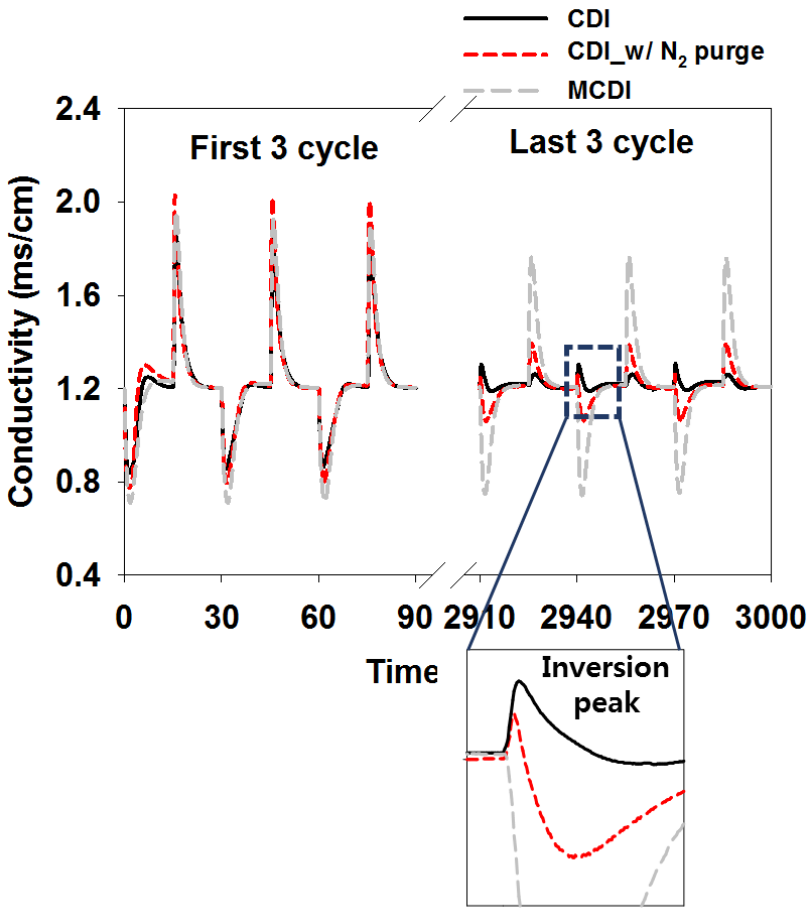

Figure 4-9. Conductivity profile at the first three cycles and the last three cycles in the long-term cycled CDI, N_2 purged CDI, and MCDI. All deionization experiments were performed twice to investigate reproducibility and presented one selected result.

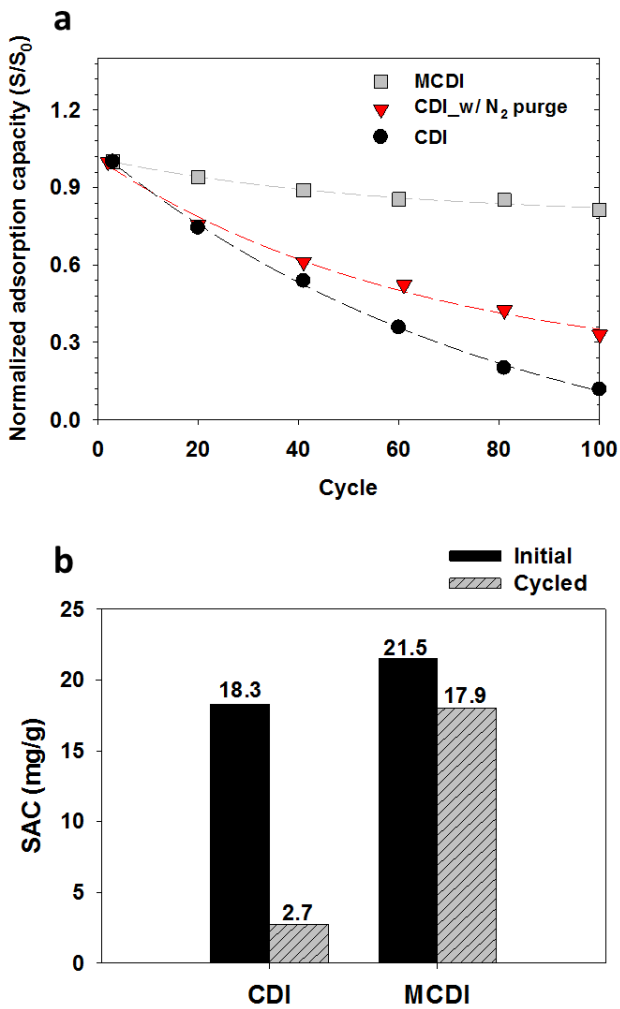

Figure 4-10. (a) Normalized salt adsorption capacity in the long-term CDI, N_2 purged CDI, and MCDI operations; (b) the salt adsorption capacity at the initial and the last step in CDI and MCDI systems. All deionization experiments were performed twice to investigate reproducibility and presented one selected result.

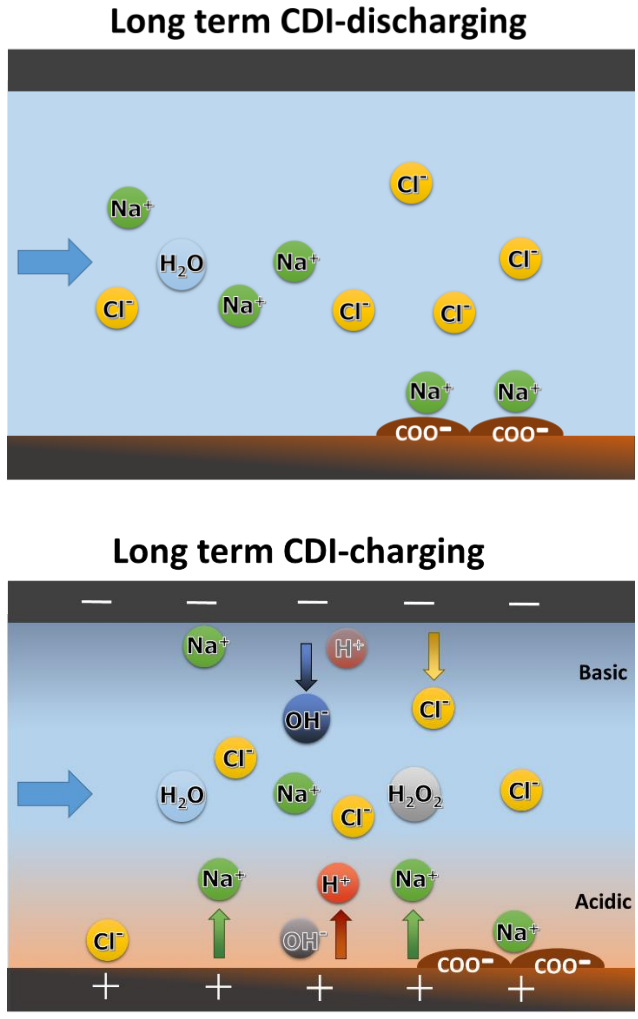

Figure 4-11. Schematic diagram of the effect of Faraday reaction products, co-ion repulsion, and oxidized anode surface on the ion adsorption performance in discharging and charging process of long-term cycled CDI system.

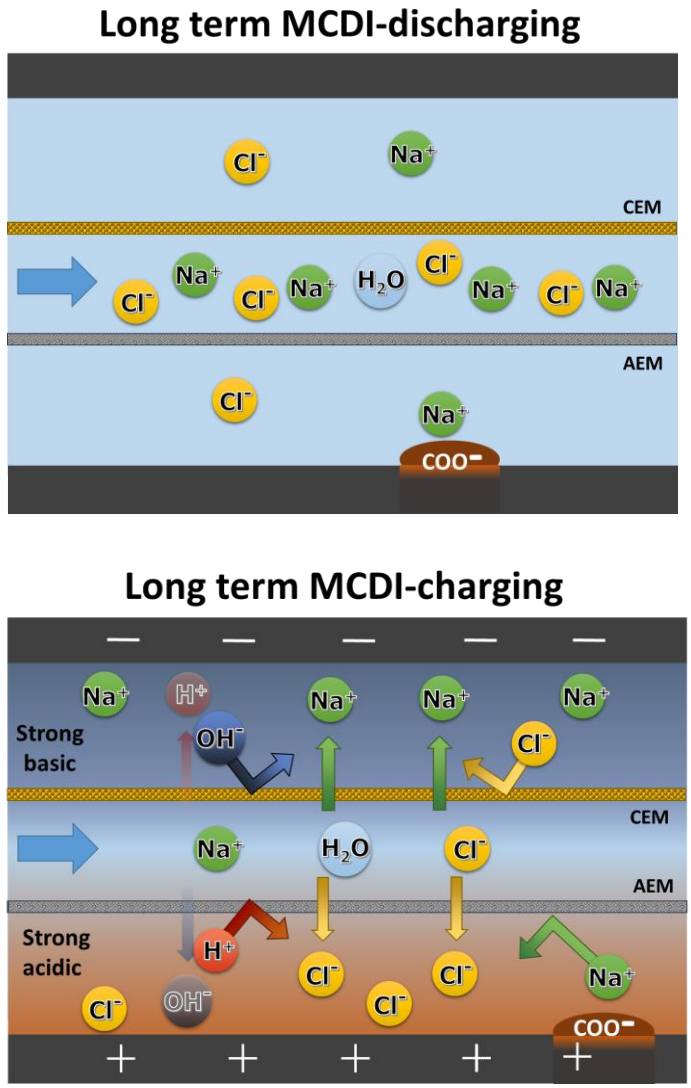

Figure 4-12. Schematic diagram of the effect of Faraday reaction products, co-ion repulsion, and little oxidized anode surface on the ion adsorption performance in discharging and charging process of long-term cycled MCDI system.

4.2.4. Change of charge consumption distribution in long-term operation

Figure 4-13 shows the quantitative analysis of the charge consumption distribution in short and long-term CDI and MCDI systems. The charge consumption distribution of CDI during the long-term operation varied greatly, while the MCDI was almost similar to the initial.

First, the charge of adsorption in the CDI system was significantly reduced from the initial 70% to the final 17%. This is because the area of charge that is consumed in addition to adsorption is increased. The most significant effect on the reduction of the charge efficiency was the co-ion repulsion, in which the initial charge consumption was 13% to the final 54%, which is higher than sum of charge for adsorption and Faradaic reaction. This remarkable increase in the co-ion repulsion charge in long-term is attributed to dominance of co-ion desorption from the oxidized electrode, as shown by the inversion region (desorption in the charging process) in the conductive profile and the interpretation (Figure 4-9 and 4-11). The charge for Faradaic reaction was also a little increased to 19% from initial 10%, which was higher than adsorption charge consumption (17%). The increase of charge consumption in Faradaic reaction was due to the constant Faradaic reaction such as the H_2O_2 generation and the pH acidification (Figure 4-2 and 4-3) despite the decrease of the total charge. The initial charge of the Faraday reaction was only about 10%, but it accumulated continuously over a long-term operation and

oxidized the anode, thus playing a key role in maximizing the co-ion repulsion charge.

Next, MCDI maintained high charge efficiency even in long-term operation. In the above, the salt adsorption capacity of MCDI was reduced by about 17% in long-term operation, but the total charge was also reduced by 17% (Figure 4-14), so the efficiency of the charge consumed by the adsorption was constant. The amount of charge consumed by the Faradaic reaction was slightly increased by the Faraday reaction, but this charge was still about 1%. Despite the partial oxidation of anode, the ion exchange membranes can control co-ion repulsion. Therefore, it was possible to maintain the high charge efficiency by preventing charge consumption for co-ion repulsion.

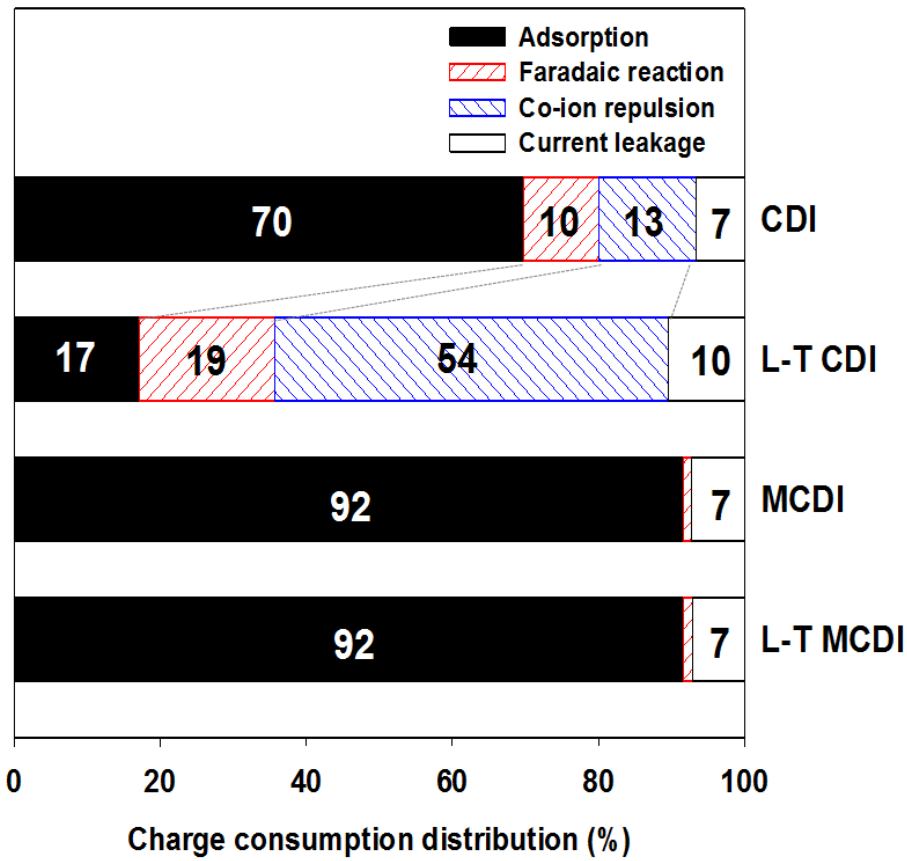

Figure 4-13. Charge consumption distribution of short and long-term CDI and MCDI systems. The charge consists of adsorption, Faradaic reaction, co-ion repulsion, and current leakages. The charge consumed in the Faradaic reaction was obtained based on the concentration of Faradaic reaction byproducts.

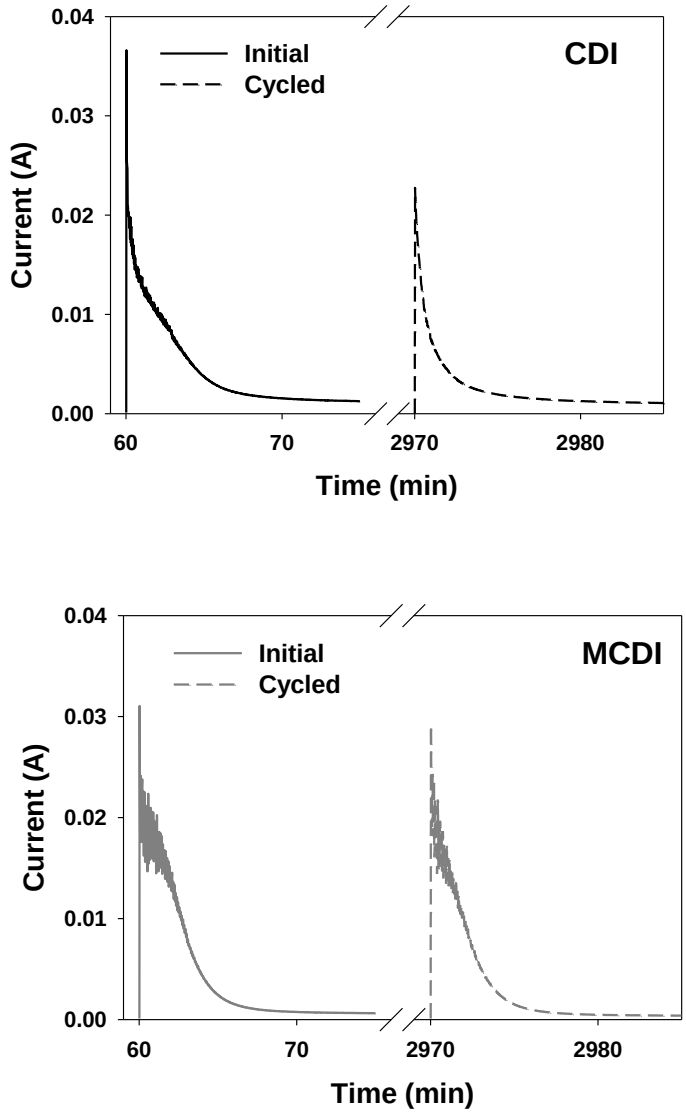

Figure 4-14. Current profiles at the initial and the last cycle in long term cycled CDI and MCDI systems. Current was used for calculation of total charge in Table 4-3.

Table 4-3. Charge consumption distribution in long-term cycled CDI and MCDI.

(Coulomb)

	C_{total}	$C_{adsorption}$	$C_{H_2O_2}$	C_{H^+}	$C_{co-ion\ repulsion}$	$C_{leakage}$
cycled CDI	**2.4**	**0.4**	**0.2**	**0.2**	**1.3**	**0.3**
cycled MCDI	**3.0**	**2.7**	**0.0**	**0.0**	**0.0**	**0.3**

$$C_{total} = C_{adsorption} + C_{Faradaic\ reaction} + C_{co-ion\ repulsion} + C_{leakage}$$

$$C_{total} = \int I \cdot dt$$

$$C_{adsorption} = \int ([NaCl]_{in} - [NaCl]_{out}) \cdot \Phi \cdot dt \cdot F$$

$$C_{Faradaic\ reaction} = C_{reduction} + C_{oxidation} \approx C_{H_2O_2} + C_{H^+}$$

$$C_{H_2O_2} = \int 2 \cdot [H_2O_2]_{out} \cdot \Phi \cdot dt \cdot F$$

$$C_{H^+} = \int_{t1}^{t2} ([H^+]_{out} - [H^+]_{peak\ pH}) \cdot \Phi \cdot dt \cdot F$$

$$C_{leakage} = (I_{residue} - I_{Faradaic\ reaction})_{at\ saturation} \cdot t$$

$$C_{co-ion\ repulsion} = C_{total} - C_{adsorption} - C_{Faradaic\ reaction} - C_{leakage}$$

$[H^+]_{peak\ pH}$ is the H^+ concentration at peak pH (the highest pH during charge); t_1 is when the pH decrease started after the peak pH; t_2 is when the end of charge; $C_{leakage}$ was obtained from leakage current at adsorption saturation based on MCDI.

4.2.5. Improvement of long-term stability by Faradaic reaction control

The MCDI system with ion exchange membrane was protected from the Faradaic reaction, resulting in a stable long-term performance. In this study, two methods of modifying the operating condition and electrode have been proposed to improve the long-term stability and interpreted in connection with Faradaic reaction. Firstly, it is performed through a control of operating condition. In the case of the CDI system, in which alternating reverse potentials were applied during the charging process, positive potentials were alternately applied to the two electrodes, resulting in symmetric oxidation. Figure 4-15 shows the FTIR spectra of long-term cycled electrodes in reverse potential applied CDI in comparison with the control. It was confirmed that the oxygen-containing functional groups were symmetrically developed in the two electrodes with the alternating reverse potentials. Figure 4-16 shows the working potential of electrodes after long-term operation with reverse potential. In contrast to Figure 4-4a, balanced distributions of anode and cathode were observed in long-term operation. Figure 4-17 shows the conductivity profile (a) and normalized SAC (b) of reverse potential applied CDI in long-term operation. CDI with alternating reverse potential produced much less reduction in desalination performance because oxidation and reduction occurred at both electrodes, maintaining the initial balanced potential distribution and symmetrical electrode characteristics. Improvement of long-term stability through applying alternate reverse potential was similarly reported in a previous study [58]. However,

oxidation of the electrodes cannot completely avoid with applying alternate reverse potential and eventually the initial performance was lost. In addition, there has been an attempt to improve the long-term performance, such as controlling the amount of DO in the feed or changing the flow type, but these also cannot prevent the electrode oxidation [28].

The following is the modification of the electrode through the ion exchange polymer (IEP) coating. The coating of IEP has been mainly used because it is cheaper than ion exchange membrane. However, this study further discussed IEP coatings in relation to Faradaic reaction and long term stability. Figure 4-18 shows the effluent pH (a) and H_2O_2 concentration (b) in the systems with IEP applied electrodes. In the case of an electrode coated with an IEP, less fluctuation in the effluent pH and generation of H_2O_2 were observed than in the case of IEP covered electrode. Figure 4-19 shows the normalized SAC of CDI system with IEP covered and coated electrode in long-term operation. The IEP film covered system showed about 61% higher stability than the control (no IEP) and the CDI with the IEP coated electrode showed 32% higher performance than that of the control. Less Faradaic reaction and stable long-term performance of IEP coating electrode can explain with less water contact of electrode. The use of ion exchange membranes can limit the transfer of oxygen and other generated Faradaic reaction products, thus it limited additional Faraday reaction. However, when an IEP coated electrode is used, the water contact reduced between the electrode and the IEP, so that the Faradaic reaction caused by the water can additionally be restricted. Carbon is

oxidized by water (Reaction 3-15), which is a key cause of long-term performance decline. Therefore, further control of water by IEP coating can contribute to prevention of oxidation of carbon electrode and improvement of long term stability. In conclusion, in order to prevent electrode oxidation and improve long-term stability, it is more effective to control or prevent surface reactions as a whole by IEP coating rather than controlling specific reactants or reactions.

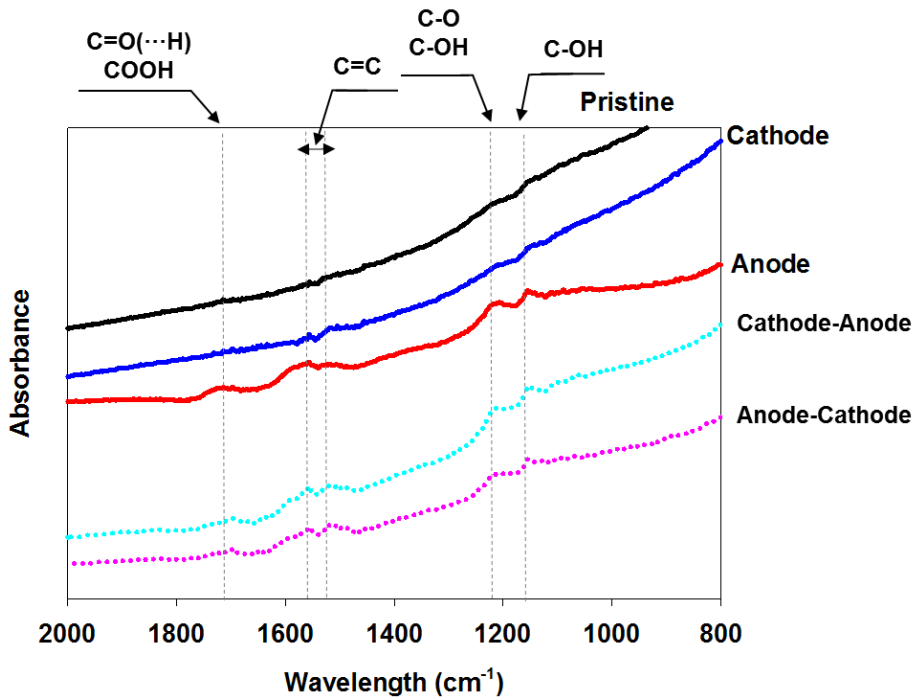

Figure 4-15. The FTIR spectra of long-term cycled electrode in reverse potential applied CDI in comparison with the control.

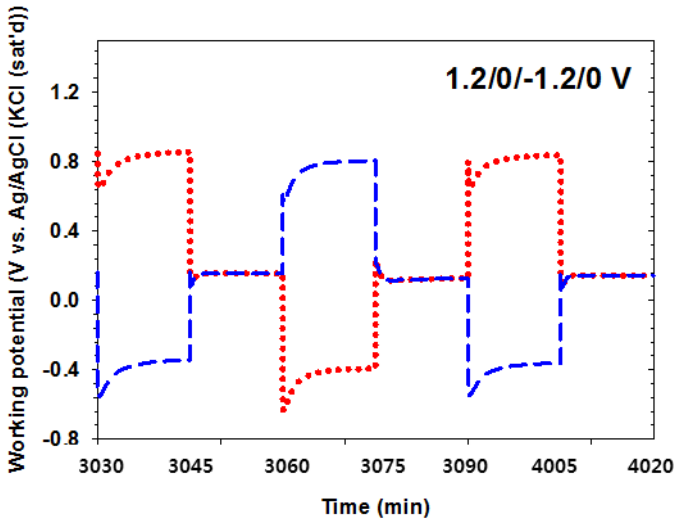

Figure 4-16. The working potentials of electrodes after long-term operation with alternated reverse potential.

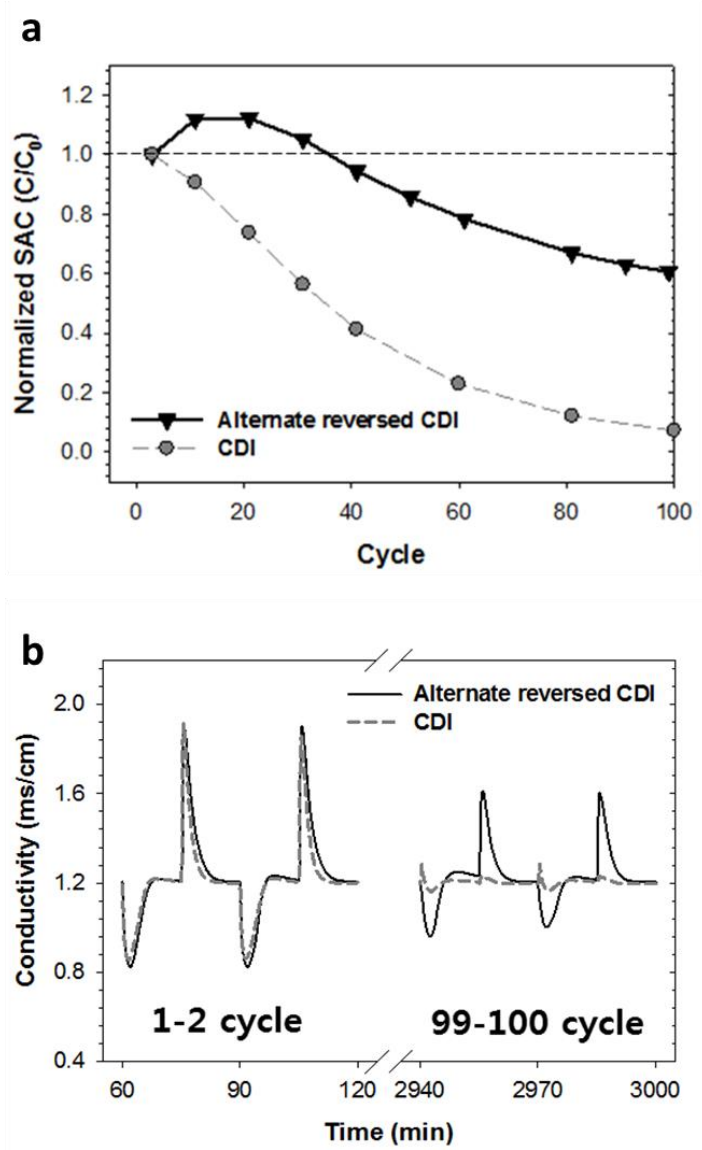

Figure 4-17. (a) The conductivity profile and (b) normalized SAC of alternate reversed potential applied CDI and the control CDI in long-term operation.

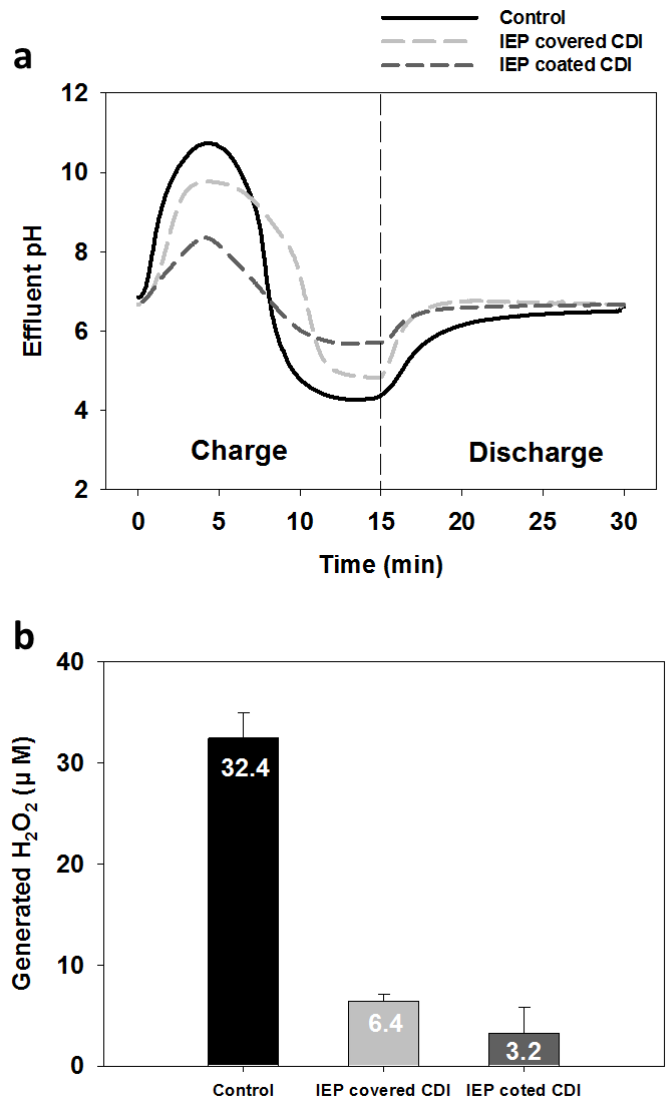

Figure 4-18. (a) The effluent pH and (b) H_2O_2 concentration of the systems with ion exchange polymer (IEP) covered or coated electrodes in comparison with the control (no IEP).

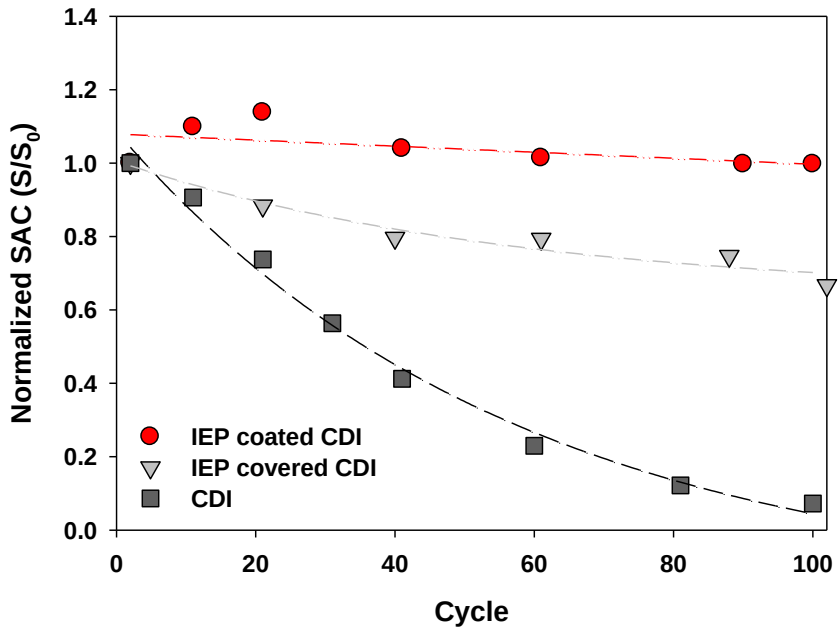

Figure 4-19. Normalized SAC of CDI systems with ion exchange polymer (IEP) covered or coated electrodes in comparison with the control (no IEP).

4.3. Summary

In long-term operation of CDI and MCDI, the changes of Faradaic reaction property was analyzed and the decrease in deionization performance was interpreted from the synergistic effects of Faradaic reaction and co-ion repulsion. The generated H_2O_2 and the acidified pH were steadily shown in long term, while the peak pH (maximum pH in charging step) decreased slightly. This is expected to be due to occurrence of additional oxidation reactions with positively shift of anode working potential. In addition, the anode was asymmetrically oxidized, especially in the CDI system, and showed a performance reduction of 85%. The oxidized surface enhances co-ion repulsion reducing desalination performance. However, in spite of partially oxidized electrodes in MCDI, co-ion repulsion could be limited by the ion-exchange membrane, which may have less impact on performance (~17% reduction). In addition, in long-term operation, the change in charge dissipation distribution was very large in CDI, but rarely in MCDI. The reason for the significant reduction in charge efficiency in CDI was the first co-ion repulsion increased to 54%, followed by the Faradaic reaction of 13%. The greatly increased co-ion repulsion was caused by the oxidized anode by the long-term accumulated Faradaic reaction. On the other hand, the MCDI system, which may be free from co-ion repulsion, could have a steady charge efficiency despite a little oxidation of anode. In addition, long-term stability improvement could be achieved through applying alternate reverse potential and IEP coating.

5. Conclusion

In this study, temporal and spatial characteristics of Faradaic reactions were analyzed and their effect on deionization performance was interpreted. Firstly, the H_2O_2 formation and pH change in case of MCDI ([H_2O_2] = 5.5 μM) were much smaller than that of CDI (37.0 μM), indicating the occurrence of less Faradaic reactions for MCDI. However, the surface pH of carbon electrode in the MCDI was much more acidic (pH ~1.5) at the anode and more basic at the cathode (pH ~ 11.7), indicating the deterred transfer of byproducts (OH^- and H^+) generated in the compartment inside of ion change membrane. The limited transfer of byproducts in the MCDI can result in depletion of the reactants (H^+, OH^-, O_2, and H_2O_2) at the surface, thereby preventing additional Faradaic reactions. In addition, the quantitative analysis regarding the extent of Faradaic reaction between these two systems were provided based on measured byproducts (H_2O_2 and H^+). The charge consumption for the Faradaic reaction was about 10% in CDI and the charge for co-ion repulsion was about 13%. Secondly, continuous Faradaic reaction phenomenon and change of desalination performance were observed in long-term operation. The long term study indicated that the performance reduction of desalination in MCDI (17% reduction) was much smaller than that of CDI (85% reduction), as supported by their asymmetrically oxidized carbon electrodes analyzed by FT-IR, CV, and XPS. The steady Faradaic reaction (19% of charge consumption) caused an asymmetric oxidation of the anode, leading to a 54% increase in co-ion

repulsion charge and a significant reduction in desalination performance. Finally, IEP coatings was suggested to improve long term stability by effectively preventing surface reactions at the electrode, including carbon oxidation by water. These results can improve the accuracy of CDI performance evaluation, especially with regard to the effect of Faradaic reactions, and contribute to the study of short term performance improvement and long term stability development.

References

[1] Y.-J. Kim, J.-H. Choi, Enhanced desalination efficiency in capacitive deionization with an ion-selective membrane, Separation and Purification Technology, 71 (2010) 70-75.

[2] S. Porada, R. Zhao, A. Van Der Wal, V. Presser, P. Biesheuvel, Review on the science and technology of water desalination by capacitive deionization, Progress in Materials Science, 58 (2013) 1388-1442.

[3] M.-W. Ryoo, G. Seo, Improvement in capacitive deionization function of activated carbon cloth by titania modification, Water Research, 37 (2003) 1527-1534.

[4] H.-J. Ahn, J.-H. Lee, Y. Jeong, J.-H. Lee, C.-S. Chi, H.-J. Oh, Nanostructured carbon cloth electrode for desalination from aqueous solutions, Materials Science and Engineering: A, 449 (2007) 841-845.

[5] J.C. Farmer, D.V. Fix, G.V. Mack, R.W. Pekala, J.F. Poco, Capacitive deionization of NaCl and NaNO3 solutions with carbon aerogel electrodes, Journal of the Electrochemical Society, 143 (1996) 159-169.

[6] L. Zou, G. Morris, D. Qi, Using activated carbon electrode in electrosorptive deionisation of brackish water, Desalination, 225 (2008) 329-340.

[7] T. Welgemoed, C. Schutte, Capacitive deionization technology™: an alternative desalination solution, Desalination, 183 (2005) 327-340.

[8] H. Li, L. Zou, L. Pan, Z. Sun, Novel graphene-like electrodes for capacitive deionization, Environmental science & technology, 44 (2010) 8692-8697.

[9] H. Li, L. Pan, T. Lu, Y. Zhan, C. Nie, Z. Sun, A comparative study on electrosorptive behavior of carbon nanotubes and graphene for capacitive deionization, Journal of Electroanalytical Chemistry, 653 (2011) 40-44.

[10] T. Kim, J. Dykstra, S. Porada, A. Van Der Wal, J. Yoon, P. Biesheuvel, Enhanced charge efficiency and reduced energy use in capacitive deionization by increasing the discharge voltage, Journal of colloid and interface science, 446 (2015) 317-326.

[11] J. Kang, T. Kim, H. Shin, J. Lee, J.-I. Ha, J. Yoon, Direct energy recovery system for membrane capacitive deionization, Desalination, 398 (2016) 144-150.

[12] J.-B. Lee, K.-K. Park, H.-M. Eum, C.-W. Lee, Desalination of a thermal power plant wastewater by membrane capacitive deionization, Desalination, 196 (2006) 125-134.

[13] A. Omosebi, X. Gao, J. Landon, K. Liu, Asymmetric Electrode Configuration for Enhanced Membrane Capacitive Deionization, ACS applied materials & interfaces, 6 (2014) 12640-12649.

[14] Y.-J. Kim, J.-H. Choi, Improvement of desalination efficiency in capacitive deionization using a carbon electrode coated with an ion-exchange polymer, Water research, 44 (2010) 990-996.

[15] P. Biesheuvel, A. Van der Wal, Membrane capacitive deionization, Journal of Membrane Science, 346 (2010) 256-262.

[16] R. Zhao, P. Biesheuvel, A. Van der Wal, Energy consumption and constant current operation in membrane capacitive deionization, Energy & Environmental Science, 5 (2012) 9520-9527.

[17] H. Li, L. Zou, Ion-exchange membrane capacitive deionization: a new strategy for brackish water desalination, Desalination, 275 (2011) 62-66.

[18] P. Biesheuvel, R. Zhao, S. Porada, A. Van der Wal, Theory of membrane capacitive deionization including the effect of the electrode pore space, Journal of Colloid and Interface Science, 360 (2011) 239-248.

[19] Y. Zhao, Y. Wang, R. Wang, Y. Wu, S. Xu, J. Wang, Performance comparison and energy consumption analysis of capacitive deionization and membrane capacitive deionization processes, Desalination, 324 (2013) 127-133.

[20] S. Porada, L. Borchardt, M. Oschatz, M. Bryjak, J. Atchison, K. Keesman, S. Kaskel, P. Biesheuvel, V. Presser, Direct prediction of the desalination performance of porous carbon electrodes for capacitive deionization, Energy Environ. Sci., 6 (2013) 3700-3712.

[21] T. Kim, J. Yoon, Relationship between capacitance of activated carbon composite electrodes measured at a low electrolyte concentration and their desalination performance in capacitive deionization, Journal of Electroanalytical Chemistry, 704 (2013) 169-174.

[22] H. Yin, S. Zhao, J. Wan, H. Tang, L. Chang, L. He, H. Zhao, Y. Gao, Z. Tang, Three-Dimensional Graphene/Metal Oxide Nanoparticle Hybrids for High-

Performance Capacitive Deionization of Saline Water, Adv. Mater., 25 (2013) 6270-6276.

[23] J.-H. Lee, W.-S. Bae, J.-H. Choi, Electrode reactions and adsorption/desorption performance related to the applied potential in a capacitive deionization process, Desalination, 258 (2010) 159-163.

[24] Y. Bouhadana, E. Avraham, M. Noked, M. Ben-Tzion, A. Soffer, D. Aurbach, Capacitive deionization of NaCl solutions at non-steady-state conditions: inversion functionality of the carbon electrodes, The Journal of Physical Chemistry C, 115 (2011) 16567-16573.

[25] I. Cohen, E. Avraham, Y. Bouhadana, A. Soffer, D. Aurbach, Long term stability of capacitive de-ionization processes for water desalination: The challenge of positive electrodes corrosion, Electrochimica Acta, 106 (2013) 91-100.

[26] J.J. Lado, R.E. Pérez-Roa, J.J. Wouters, M.I. Tejedor-Tejedor, M.A. Anderson, Evaluation of operational parameters for a capacitive deionization reactor employing asymmetric electrodes, Sep. Purif. Technol., 133 (2014) 236-245.

[27] S. Maass, F. Finsterwalder, G. Frank, R. Hartmann, C. Merten, Carbon support oxidation in PEM fuel cell cathodes, Journal of Power Sources, 176 (2008) 444-451.

[28] I. Cohen, E. Avraham, Y. Bouhadana, A. Soffer, D. Aurbach, The effect of the flow-regime, reversal of polarization, and oxygen on the long term stability in capacitive de-ionization processes, Electrochimica Acta, 153 (2015) 106-114.

[29] X. Gao, A. Omosebi, J. Landon, K. Liu, Dependence of the capacitive deionization performance on potential of zero charge shifting of carbon xerogel electrodes during long-term operation, Journal of The Electrochemical Society, 161 (2014) E159-E166.

[30] D. He, C.E. Wong, W. Tang, P. Kovalsky, T.D. Waite, Faradaic Reactions in Water Desalination by Batch-Mode Capacitive Deionization, Environmental Science & Technology Letters, 3 (2016) 222-226.

[31] W. Tang, D. He, C. Zhang, P. Kovalsky, T.D. Waite, Comparison of Faradaic reactions in capacitive deionization (CDI) and membrane capacitive deionization (MCDI) water treatment processes, Water Research, (2017) 229-237.

[32] B. Shapira, E. Avraham, D. Aurbach, Side Reactions in Capacitive Deionization (CDI) Processes: The Role of Oxygen Reduction, Electrochimica Acta, 220 (2016) 285-295.

[33] P. Nativ, Y. Badash, Y. Gendel, New insights into the mechanism of flow-electrode capacitive deionization, Electrochemistry Communications, (2017) 24-28

[34] M.A. Anderson, A.L. Cudero, J. Palma, Capacitive deionization as an electrochemical means of saving energy and delivering clean water. Comparison to present desalination practices: Will it compete?, Electrochimica Acta, 55 (2010) 3845-3856.

[35] R. Zhao, S. Porada, P. Biesheuvel, A. Van der Wal, Energy consumption in membrane capacitive deionization for different water recoveries and flow rates, and comparison with reverse osmosis, Desalination, 330 (2013) 35-41.

[36] H. Yin, S. Zhao, J. Wan, H. Tang, L. Chang, L. He, H. Zhao, Y. Gao, Z. Tang, Three-dimensional graphene/metal oxide nanoparticle hybrids for high-performance capacitive deionization of saline water, Advanced materials, 25 (2013) 6270-6276.

[37] S. Porada, L. Weinstein, R. Dash, A. Van Der Wal, M. Bryjak, Y. Gogotsi, P. Biesheuvel, Water desalination using capacitive deionization with microporous carbon electrodes, ACS applied materials & interfaces, 4 (2012) 1194-1199.

[38] E. Avraham, Y. Bouhadana, A. Soffer, D. Aurbach, Limitation of charge efficiency in capacitive deionization I. on the behavior of single activated carbon, Journal of the Electrochemical Society, 156 (2009) 95-99.

[39] Y. Bouhadana, M. Ben-Tzion, A. Soffer, D. Aurbach, A control system for operating and investigating reactors: the demonstration of parasitic reactions in the water desalination by capacitive de-ionization, Desalination, 268 (2011) 253-261.

[40] K. Kinoshita, Carbon: electrochemical and physicochemical properties, Wiley, 978-0-471-84802-8, (1988).

[41] E. Yeager, Electrocatalysts for O 2 reduction, Electrochimica Acta, 29 (1984) 1527-1537.

[42] F. Rodríguez-Reinoso, The role of carbon materials in heterogeneous catalysis, Carbon, 36 (1998) 159-175.

[43] Y. Oren, Capacitive deionization (CDI) for desalination and water treatment—past, present and future (a review), Desalination, 228 (2008) 10-29.

[44] X. Gao, A. Omosebi, J. Landon, K. Liu, Enhancement of charge efficiency for a capacitive deionization cell using carbon xerogel with modified potential of zero charge, Electrochemistry Communications, 39 (2014) 22-25.

[45] E. Avraham, M. Noked, I. Cohen, A. Soffer, D. Aurbach, The dependence of the desalination performance in capacitive deionization processes on the electrodes PZC, Journal of the Electrochemical Society, 158 (2011) P168-P173.

[46] X. Gao, A. Omosebi, J. Landon, K. Liu, Surface charge enhanced carbon electrodes for stable and efficient capacitive deionization using inverted adsorption–desorption behavior, Energy & Environmental Science, 8 (2015) 897-909.

[47] E. Avraham, M. Noked, Y. Bouhadana, A. Soffer, D. Aurbach, Limitations of charge efficiency in capacitive deionization II. On the behavior of cdi cells comprising two activated carbon electrodes, Journal of the Electrochemical Society, 156 (2009) 157-162.

[48] E. Avraham, M. Noked, Y. Bouhadana, A. Soffer, D. Aurbach, Limitations of charge efficiency in capacitive deionization processes III: The behavior of surface oxidized activated carbon electrodes, Electrochimica Acta, 56 (2010) 441-447.

[49] J. Kang, T. Kim, K. Jo, J. Yoon, Comparison of salt adsorption capacity and energy consumption between constant current and constant voltage operation in capacitive deionization, Desalination, 352 (2014) 52-57.

[50] A.N. Baga, G. Johnson, N.B. Nazhat, R.A. Saadalla-Nazhat, A simple spectrophotometric determination of hydrogen peroxide at low concentrations in aqueous solution, Analytica chimica acta, 204 (1988) 349-353.

[51] J.-H. Choi, Determination of the electrode potential causing Faradaic reactions in membrane capacitive deionization, Desalination, 347 (2014) 224-229.

[52] J. Liu, M. Lu, J. Yang, J. Cheng, W. Cai, Capacitive desalination of ZnO/activated carbon asymmetric capacitor and mechanism analysis, Electrochimica Acta, 151 (2015) 312-318.

[53] T. Kim, J. Yu, C. Kim, J. Yoon, Hydrogen peroxide generation in flow-mode capacitive deionization, Journal of Electroanalytical Chemistry, 776 (2016) 101-104.

[54] H. Li, Y. Gao, L. Pan, Y. Zhang, Y. Chen, Z. Sun, Electrosorptive desalination by carbon nanotubes and nanofibres electrodes and ion-exchange membranes, Water research, 42 (2008) 4923-4928.

[55] P. Srimuk, L. Ries, M. Zeiger, S. Fleischmann, N. Jäckel, A. Tolosa, B. Krüner, M. Aslan, V. Presser, High performance stability of titania decorated carbon for desalination with capacitive deionization in oxygenated water, RSC Advances, 6 (2016) 106081-106089.

[56] X. Gao, J. Landon, J.K. Neathery, K. Liu, Modification of carbon xerogel electrodes for more efficient asymmetric capacitive deionization, Journal of The Electrochemical Society, 160 (2013) E106-E112.

[57] J.-S. Kim, J.-H. Choi, Fabrication and characterization of a carbon electrode coated with cation-exchange polymer for the membrane capacitive deionization applications, Journal of membrane science, 355 (2010) 85-90.

[58] X. Gao, A. Omosebi, N. Holubowitch, J. Landon, K. Liu, Capacitive deionization using alternating polarization: effect of surface charge on salt removal, Electrochimica Acta, 233 (2017) 249-255.

국문초록

축전식 탈염 (Capacitive deionization: CDI)기술은 다공성 활성탄 전극 사이에 전위차를 인가하여 염수의 염을 제거하는 담수화 공정이다. 막 축전식 탈염 (MCDI)공정은 이온교환막을 전극 사이에 추가로 장착하여 담수화 용량을 향상시킨 가장 널리 사용되는 CDI 시스템이다. 축전식 탈염기술은 Non Faradaic 반응에 의해 주로 탈염이 이루어 지는 것으로 알려져 있으나 최근에는 과산화수소 생성과 pH 변화와 그리고 탄소 전극의 산화와 관련한 Faradaic 반응에 대해 제한적인 보고가 있었다. 따라서 CDI 와 MCDI 시스템에서 Faradaic 반응특성에 대한 심층적인 연구가 요구된다.

본 연구는 CDI 와 MCDI 시스템에서 Faradaic 반응의 특성과 담수화 성능에 끼치는 영향을 정략적으로 분석 하고자 하였다. 주요 연구 결과로써, 첫 번째는 과산화 수소의 발생 및 유출수 pH 의 변화가 CDI 대비 (과산화수소 ~37.0 μM) MCDI (~5.5 μM)에서 훨씬 적었으며, 이는 MCDI 에서 패러데이 반응이 적게 발생함을 의미한다. 반면, MCDI 시스템에서 전극 표면의 pH 는 CDI 대비 양극에서 보다 강한 산성을 띄고 (pH~1.5) 음극에서 강한 염기성을 띄었으며 (pH~11.7), 이는 MCDI 의 이온교환막에 의하여 발생된 반응 부산물들(수소이온과 수산화이온)의 이동이 제한되기 때문으로 설명될 수

있었다. 두 번째로, 장기운전 연구 결과에 따르면, MCDI(~17%)에서의 담수화 성능 감소는 CDI(~85%)보다 훨씬 적었으며, 이는 장기 운전된 전극의 FT-IR, CV 와 XPS 분석 결과 비대칭적으로 산화된 양극에 의하여 야기될 수 있었다. 또한, 장기 성능감소를 극복하기 위한 전략으로 이온교환수지의 코팅과 교차전위 인가 방법이 제안되었다. 마지막으로, 본 연구를 통한 단기 또는 장기 담수화 성능에 영향을 끼치는 Faradaic 반응에 대한 보다 깊은 이해는 궁극적으로 CDI 성능 및 장기 안정성 향상 연구에 기여할 수 있을 것이다.

주요어: 축전식 탈염공정, 담수화, Faradaic 반응, pH 분포, 과산화수소, 탄소전극 산화, 전하 소비

학 번: 2010-24100